UNIVERSIDADE D
COIMBRA

João Manuel Carrilho Gil Martins

Time Interleaved Block Windowed Burst OFDM
Channel Estimation and Synchronization Techniques

Dissertação no âmbito do Mestrado Integrado em Engenharia Eletrotécnica e de Computadores, ramo de especialização em Telecomunicações, orientada pelo Professor Doutor Marco Alexandre Cravo Gomes e pelo Professor Doutor Vitor Manuel Mendes da Silva e apresentada à Faculdade de Ciências e Tecnologia da Universidade de Coimbra no Departamento de Engenharia Eletrotécnica e de Computadores.

Outubro 2020

UNIVERSIDADE D
COIMBRA

Time Interleaved Block Windowed Burst OFDM: Channel Estimation and Synchronization Techniques

João Manuel Carrilho Gil Martins

Dissertação para obtenção do Grau de Mestre em
Engenharia Electrotécnica e de Computadores

Orientador:	Doutor Marco Alexandre Cravo Gomes
Co-Orientador:	Doutor Vitor Manuel Mendes da Silva

Júri

Presidente:	Doutor Fernando Manuel dos Santos Perdigão
Orientador:	Doutor Marco Alexandre Cravo Gomes
Vogal:	Doutor Luís Alberto da Silva Cruz

Outubro de 2020

With regard to performance, commitment, effort, dedication, there is no middle ground. Or you do something very well or not at all.

- Ayrton Senna

Do not be afraid of getting lost ... the more we give of ourselves, the more we will find ourselves.

- Pope John Paul II

Agradecimentos

Em primeiro lugar, quero prestar um agradecimento muito especial aos meus orientadores, Doutor Marco Gomes e Doutor Vitor Silva pela ajuda, profissionalismo, motivação e total disponibilidade durante todo o desenrolar desta dissertação. Foi uma honra puder aprender e trabalhar ao vosso lado.

Em segundo, agradeço ao DEEC/UC, em particular ao corpo docente, por todos os conhecimentos transmitidos que me formaram e que me deram as bases para o profissional que sou hoje. E claro, aos elementos não docentes e funcionários que diariamente mantive contacto e dão vida ao nosso Departamento.

Agradeço ao Instituto de Telecomunicações pela oportunidade concedida e por todas as condições fornecidas.

Um agradecimento à malta do IT que tornaram a minha estadia no laboratório mais agradável, em especial ao Carlos e ao Óscar. Ao Filipe, pelo colega que encontrei e pude partilhar conhecimento. Por toda a ajuda prestada e paciência para aturar as minhas dúvidas durante a realização desta dissertação. O meu sincero obrigado!

Àquela que foi, durante muitos anos, a minha segunda casa. Ao NEEEC/AAC. Por aprender que o errar e o sucesso na vida depende quase sempre do empenho e trabalho que exigimos de nós próprios. Por aprender o significado de cooperação, respeito, sentido de responsabilidade e trabalho em equipa. A todas as pessoas com quem lidei, devo uma palavra de agradecimento, em especial à Ana, André, Bento, Bruno, Ivo, Miguel e Ruben.

Aos meus grandes amigos alentejanos agradeço pelas memórias, amizade e constante ligação, apesar da distância. Fica, novamente, a promessa que brevemente vos faço uma visita a todos. Ao incrível Nelson, que apesar do pouco juízo, é um grande camarada.

Aos amigos que Coimbra me deu e estiveram presentes neste percurso: ao Abegão, Afonso, Baltazar, Henriques, Jorge, Rui Gouveia, Rui Silva, Moisés e Poço. Ao Marco Silva pelo companheirismo, esforço na revisão dos acrónimos deste documento e por ”pregrarmos” um fim às nossas teses. Ao Zé Pedro pela motivação, apoio, boa disposição e experiências. Pelo espírito de companheirismo e disponibilidade em todos os momentos que me fez crescer como colega e amigo.

Por fim, quero demonstrar o meu forte agradecimento aos meus pais e irmão pela oportunidade, formação, crença nas minhas capacidades e pelo apoio incondicional que me deram durante esta longa caminhada.

Um especial carinho, agradecimento e amor para a Leo, que me deu motivação e disposição e soube ser sempre compreensiva comigo nos momentos mais difíceis. Pelo lugar que representa na minha vida e por acabarmos juntos esta última etapa na Universidade de Coimbra.

A todos aqueles que influenciaram o meu percurso académico,
Muito Obrigado!

Este trabalho foi financiado pela FCT/MEC através de fundos nacionais e quando aplicável co-financiado pelo FEDER - PT2020 no âmbito do projeto UID/EEA/50008/2019 e PES3N (2018-SAICT-45-2017-POCI-01-0145-FEDER-030629) e MASSIVE5G (POCI-01-0145-FEDER-030588).

Abstract

In the segment of communications industry, wireless mobile communications are one of the most important innovations of our times due to its impact in the global economy and society. Expectations grow with the arrival and demands that the fifth generation of mobile telecommunications (5G) brings associated with an everywhere user access with better reliability and quality. In this context, *Orthogonal Frequency Division Multiplexing* (OFDM) is a widely used system that guarantees robustness against frequency selectivity channels, provide high data transmission rates and a easy implementation based on the discrete Fourier transform. However, this technique has high limited spectral efficiency, low power efficiency and sensitivity to synchronization errors. As an alternative, hybrid modulation techniques such as the time interleaved block windowed burst orthogonal frequency division multiplexing (TIBWB-OFDM) were developed.

This thesis develops the TIBWB-OFDM transceiver model and the modifications necessary to implement this technique in a real wireless link scenarios. Hence, channel estimation and frame synchronization algorithms were the key challenges and focus of this work. An important step to achieve reliable frame synchronization is the choice of preamble sequences with optimum correlation proprieties, such as the Zadoff-Chu (ZC) sequences. Our experimental results show that by applying a correlation algorithm and a threshold device it is possible to detect perfectly each TIBWB-OFDM frame beginning. On the other hand, ZC sequences were also used to acquire the channel information by applying estimators and algorithms based on the OFDM technique.

Therefore, this thesis proposes a joint channel and frame synchronization estimation using power amplified ZC sequences as preambles in the TIBWB-OFDM method.

Keywords

Channel Estimation, Cross-Correlation, Frame Synchronization, Zadoff-Chu (ZC) sequences, Time Interleaved Block Windowed Burst Orthogonal Frequency Division Multiplexing (TIBWB-OFDM)

Resumo

No contexto da indústria de telecomunicações, as comunicações móveis desempenham um papel muito importante devido ao seu impacto na economia e na sociedade global. As expectativas aumentam com a introdução da quinta geração (5G) que permite o acesso dos utilizadores em qualquer lugar com elevada fiabilidade e qualidade de serviço. Dentro deste contexto, é usado o *Orthogonal Frequency Division Multiplexing* (OFDM) que garante robustez contra canais seletivos no domínio da frequência, fornece elevadas taxas de transmissão de dados e fácil implementação baseada na transformada discreta de Fourier. No entanto, esta técnica apresenta uma eficiência espectral limitada, baixa eficiência energética e sensibilidade a erros de sincronismo. Como alternativa, foram desenvolvidas técnicas de modulação híbridas, como o *Time Interleaved Block Windowed Burst-OFDM* (TIBWB-OFDM).

Esta dissertação desenvolve o modelo do transceptor TIBWB-OFDM através da introdução de técnicas adequadas a um cenário de comunicações reais sem fios. Consequentemente, os principais desafios e foco deste trabalho passaram pelo desenvolvimento de algoritmos de estimação de canal e sincronismo de tramas. Um passo importante para obter uma sincronização de tramas fiável é a escolha de preâmbulos com propriedades de correlação ótimas, como por exemplo, as sequências de Zadoff-Chu (ZC). Os resultados experimentais mostram que aplicando algoritmos de correlação e um dispositivo de limiar, é possível detectar perfeitamente o ínicio de cada trama TIBWB-OFDM. Em simultâneo, as sequências de ZC foram também aplicadas no contexto de estimação de canal através da aplicação de estimadores e algoritmos desenvolvidos baseados no OFDM.

Desta forma, esta dissertação propõe um método conjunto de estimação de canal e sincronismo de tramas, aplicado ao TIBWB-OFDM, tomando partido das sequências ZC amplificadas.

Palavras Chave

Correlação Cruzada, Estimação de Canal, Sincronismo de trama, Sequências de Zadoff-Chu (ZC), *Time Interleaved Block Windowed Burst Orthogonal Frequency Division Multiplexing* (TIBWB-OFDM)

Contents

List of Figures

List of Acronyms

AWGN additive white gaussian noise

BWB-OFDM block windowed burst orthogonal frequency division multiplexing

BER bit error rate

CAZAC constant amplitude zero auto correlation

CFR channel frequency response

CIR channel impulse response

CFO carrier frequency offset

CSI channel state information

CP cyclic prefix

DFT discrete fourier transform

FDE frequency domain equalization

FFT fast fourier transform

FF filter feedforward filter

FB filter feedback filter

IBI inter-block interference

ICI inter-carrier interference

IDFT inverse discrete fourier transform

IFFT inverse fast fourier transform

ISI inter-symbol interference

IB-DFE iterative block decision feedback equalization

I/Q In-phase and Quadrature

LTE long term evolution

LoS line of sight

LLR log-likelihood ratio

LO local oscillators

LS least-square

LMMSE linear minimum mean square error

MC multi-carrier

MMSE minimum mean square error

MIMO multiple input multiple output

OOB out of band

OFDM orthogonal frequency division multiplexing

P/S parallel to serial

PAPR peak-to-average power ratio

PSD power spectral density

PSS primary synchronization signal

QPSK quadrature phase shift keying

SC single-carrier

S/P serial to parallel

SRRC square root raised cosine

SNR signal-to-noise ratio

SISO single input single output

SDR software defined radio

SSS secondary synchronization signal

SCO sampling clock offset

TDE Time Domain Equalization

TIBWB-OFDM time interleaved block windowed burst orthogonal frequency division multiplexing

TIBWB-OFDM WTO TIBWB-OFDM with windowing time overlapping

WTO windowing time overlapping

ZC Zadoff – Chu

ZP zero-pad

ZF zero-forcing

Notation Summary

Mathematical notations are listed below in the respective order:

$\mathbf{A^T}$	conjugate-transpose matrix
$\mathbf{A}^*$	complex conjugate matrix
$\mathbf{A^{-1}}$	inverse matrix
$\mathbf{diag}(\mathbf{A})$	diagonal matrix
$[\mathbf{A}]_{\mathbf{m,n}}$	the matrix element in m^{th} row and n^{th} column
$\mathbf{a_m}$	the m^{th} vector
$\mathbf{A_m}$	the m^{th} matrix
$\odot$	element-wise multiplication between two matrices
$\Re$	real part
$\Im$	imaginary part
$\mathbf{E}(\cdot)$	Mathematical expectation / mean value

Matrices and vectors are denoted with boldface letters. Upper letters will be used for representing frequency domain variables and lower letters for time domain variables.

1

Introduction

Contents

The progressive growth of mobile communications services and the challenges leveraged by new technologies, among which the next generations of communications, namely the Fifth Generation (5G) and beyond 5G, tries to answer the necessity to provide a wide range of user velocities, high data rates, high spectral and power efficiency and reliability to transmit data under adverse channel conditions.

1.1 Motivation

Orthogonal Frequency Division Multiplexing (OFDM) is one of the most famous modulation techniques in the telecommunications industry. Used in the 4^{th} mobile generation long term evolution (LTE) and proposed as a reference technology for 5G systems [7], OFDM provides high data transmissions rates while holding a functional low computational complexity communication system. It uses the discrete fourier transform (DFT), a breakthrough in OFDM's history, since this eliminated the need for a bank of subcarrier oscillators, thus opening the way for an easier, more useful, and efficient system implementation [8]. Unlike conventional single-carrier (SC) techniques, where each symbol occupies the whole transmission bandwidth, the in-built serial to parallel (S/P) conversion of this multi-carrier (MC) scheme offers a delay spread protection, which can be extended by using a cyclic prefix (CP) larger than the channel delay spread, avoiding inter-symbol interference (ISI). Also, the lower data rate OFDM frequency domain subcarriers maintain the orthogonality propriety if the spacing between them is set to the inverse sampling period among consecutive subcarriers. By ensuring this, it is possible to avoid inter-carrier interference (ICI) [5].

However, despite being a robust technique, these OFDM advantages come at the price of limited spectral, low power efficiency and sensitivity to synchronization errors. Also, the peak-to-average power ratio (PAPR) increases with the number of used OFDM subcarriers, a non-desirable factor since it influences the power amplifier's design and efficiency being the main limitation to the energy efficiency of OFDM-based communication systems. Errors in both timing and frequency synchronizations introduce additional interference to the OFDM systems which ultimately degrade the performance [5]. Proper channel estimation is a key part of any communication link which is severely affected by timing synchronization in OFDM [9]. A wide variety of techniques have been proposed for the effective estimation and correction of both timing and carrier frequency errors at the OFDM receiver.

As an alternative, hybrid modulation techniques such as the block windowed burst orthogonal frequency division multiplexing (BWB-OFDM) [1] were devel-

oped, and more recently the time interleaved block windowed burst orthogonal frequency division multiplexing (TIBWB-OFDM) [2]. Methods for achieving better bit error rate (BER) performance and increase spectral efficiency are also explored in the latter modulation technique. More specifically, the use of non-linear equalization algorithms, such as the iterative block decision feedback equalization (IB-DFE) [3] and exploring new block windowing techniques with windowing time overlapping (WTO) [4]. However, the scientific research conducted so far in the development of these hybrid models assumed that the receiver is perfectly synchronized and has complete knowledge of the channel, that is, all the channel state information (CSI) was fully known *a priori*, something that in a real communication system scenario does not happen.

Channel estimation and timing and frequency synchronization are in fact, two of the most important challenges to deal in the practical deployment on any wireless systems since the signal that travels between the transceiver radio channel can be highly dynamic, which corrupts the transmitted data and limits the system performance [10]. However, as long as the receiver is able to accurately estimate these channels modifications it is possible to recover reliable information. For that, the most usual approach in OFDM-based systems are either inserting known pilot symbols in the transmitted frame or training sequences. Still, the topic of synchronization and channel estimation remains open in the TIBWB-OFDM systems, for which solutions based on conventional OFDM system are not straightforward extendable.

1.2 Objectives

This dissertation aims to provide an insight of how the TIBWB-OFDM would perform in a more realistic and practical scenario. For that, it is important to predict, in a simulated and controlled environment, how this implementation would perform, addressing the needs in a new assembled TIBWB-OFDM architecture: by incorporating good correlation training sequences, like the Zadoff – Chu (ZC) sequences, on the block burst transceivers schemes for proper and reliable channel estimation algorithms and frame synchronization in a single input single output (SISO) system.

1.3 Contributions

Using a joint channel estimation and frame synchronization through a power amplified Zadoff-Chu (ZC) preamble sequence can offer a close output performance comparatively to the achieved with perfect channel state information (CSI). Hence, this dissertation offers a number of OFDM based techniques that could perform well in the TIBWB-OFDM system, including the pilot-type allocation strategy, the

channel estimators for a linear equalizer receiver structure or by adapting the iterative block decision feedback equalization (IB-DFE) structure and frame correlators algorithms.

This work also gives the basics for a direct possible application of the proposed TIBWB-OFDM architecture in a practical testbed deployment, through a *Matlab* code implementation target to an SDR employment.

1.4 Dissertation Outline

This dissertation's remaining structure is organized as follows: Chapter 2 introduces the background knowledge of typical wireless channels and different modulation techniques, specifically for new alternative hybrid communications systems, which will be the foundation for this work. Chapter 3 starts by addressing special attention for coherent detection, symbol equalization, synchronization and channel estimation techniques which are essential in the designing of a receiver. Chapter 4 presents the new proposed TIBWB-OFDM's joint channel estimation and frame synchronization strategy based on the use of ZC sequences, along with a set of adapted iterative equalizers. The simulations conducted a discussion and analysis of the obtained results are also presented in this Section. Finally, Chapter 5 concludes this dissertation and presents some future work proposals.

2

Wireless Communications

Contents

2.1 Introduction

In this chapter, an overview of all the relevant scientific knowledge required to provide a clearer perspective of the work carried in this dissertation is given. The reader is also provided a step-by-step progression of the different hybrid modulation techniques necessary for the final system implementation.

2.2 Characterization of Propagation Channels

Typically, a wireless communications system consists of three parts: the transmitter (Tx), receiver (Rx) and the wireless channel. As expected, the first two elements can be designed to provide a system with a better tradeoff between reliability and efficiency. However, the wireless channel cannot be engineered, and it is characterized by two kind of inevitable variations: large-scale fading, due to path loss (P) and shadowing (S), and small-scale fading, due to the multipath fading (h) [11].

2.2.1 Large-scale fading

The simplest path-loss model corresponds to a free space propagation line of sight (LoS) scenario. Based on the Friis transmission equation it is possible to relate the transmitted power (Pt) and received power (Pr) between two antennas in a LoS link separated by a distance D, where

$$\frac{Pr}{Pt} = \left(\frac{\lambda}{4\pi D}\right)^2 G_{0t} G_{0r}, \tag{2.1}$$

where G_{0t} and G_{0r} represent the transmitted and received gains respectively and λ the wavelength of the radio carrier [12]. Therefore, by the previous (2.1), it is possible to conclude that under free space propagation the received power from radio signals decreases as the square of the distance between the transmitter and receiver. Also, the shorter the carrier wavelength, λ, the higher the path loss.

The Shadowing effect (S) takes in consideration the random signal variations caused by the presence of obstacles between the propagation path. This phenomenon is usually modeled as a log-normal distribution and is given by:

$$f_{\Omega_p}(x) = \frac{10}{x\sigma_{\Omega_p}(x)\sqrt{2\pi}\ln 10} \times e^{-\frac{(10\log_{10}x-\mu_{\Omega_p})^2}{2\sigma^2_{\Omega_p}}}, \tag{2.2}$$

where Ω_p represents the mean-squared envelope level, μ_{Ω_p} the mean and σ_{Ω_p} the standard deviation of the shadowing effect [11].

2.2.2 Small-scale fading

In a real urban environment, wireless signals rarely experience from LoS propagation since the presence of local scatters cause the direct radio signal between the transceivers to be obstructed (non-LoS) causing the signals to propagate through phenomena like reflection, diffraction or scattering resulting in a delayed received signal with distinctive arrival paths, also referred as the delay spread [13].

In other words, the wireless system is affected by the multipath fading and can be modeled as a linear time-varying system. Assuming that the time-varying channel impulse response (CIR) of a wireless channel can be modeled as the superposition of L resolvable paths or taps, then, the time-varying impulse response of the channel can be expressed as

$$h(\tau;t) = \sum_i \alpha(t) e^{-j\theta_i(t)} \delta(\tau - \tau_i), \tag{2.3}$$

where τ_i is the delay of the *i-th* path, $\alpha(t)$ is the corresponding complex amplitude, and $\delta(\tau)$ is the dirac impulse function [13].

2.2.3 Coherence Bandwidth and ISI effect

Another important aspect of channel modeling is its behavior when transmitting different signals which can suffer either flat or frequency-selective fading depending on the coherence bandwidth of the wireless channel, B_c, and the respectively transmitted signal bandwidth, B. If B_c is large in comparison with B, then we are in a scenario where the channel fading is approximately equal across the entire signal bandwidth, and therefore it suffers from flat fading causing the channel to experience negligible ISI. On the other hand, if B_c is small in comparison with B, then the signal is severely distorted by the channel suffering from frequency selective fading and experiencing significant ISI, degrading the overall system performance.

Note that, the signal bandwidth B is inversely proportional to the symbol time T_b. So, in order to avoid the effect of ISI, it is important to guarantee a symbol rate (where $Rb = \frac{1}{T_b}$) below the *Nyquist* rate of 2 times the signal bandwidth, i.e., B is at least equal to $\frac{R_b}{2}$ [14].

2.3 Modulation Techniques

In wireless communications, there are two main transmission categories in digital modulation: single-carrier (SC) and multi-carrier (MC) transmission. Bearing in mind that future telecommunication systems must support several high data rate users, the use of conventional SC transmission systems will inevitably cause a delay

spread much higher than the symbol duration which causes ISI. To try to suppress this effect, a very complex receiver structure must be engineered, mainly by computational expensive equalization and channel estimation algorithms to correctly recover the transmitted data. To that end, MC modulation appeared as the solution for solving this dilemma. The basic idea of this approach is to divide the transmitted data into N different low rate sub-streams and send these over different sub-channels centered at different subcarrier frequencies, causing the symbol duration to be larger than the delay spread preventing any ISI phenomenon to happen. Therefore, in this scenario, the wireless channel can be considered as a flat fading channel and thus easier to be estimated and straightforward equalized [8, 14].

It should be reasonable to think that by increasing the number of subcarriers, then the overall system should perform better because it could handle more extensive delay spreads. However, it is essential to achieve a reasonable trade-off since having the subcarrier frequencies very close to each other originates possible interference among adjacent sub-channels, i.e., inter-carrier interference (ICI). Additionally, it makes the synchronization process very challenging, where a slight carrier frequency offset can cause a significant frequency mismatch between adjacent subcarriers [8].

So in order to avoid ICI, it is essential to add a guard interval between each adjacent subcarrier at the expense of reducing spectral efficiency. However, the spectrum can be improved by carefully choosing the spacing between carriers, ensuring their orthogonality and allowing overlapping between independently subchannels. It was based on these concepts that orthogonal frequency division multiplexing (OFDM), one of the most decisive multi-carrier modulation techniques and adopted in several communications standards, was developed.

2.4 Orthogonal Frequency Division Multiplexing

OFDM is a unique method of MC transmission, and it has become the predominant modulation technique in modern digital transmission systems such as European digital audio broadcasting (DAB) system, European digital video broadcasting terrestrial transmission (DVB-T) system, asymmetric digital subscriber line (ADSL), wireless local area network (WLAN), broadband wireless access network (BWA), worldwide interoperability for microwave access (WiMAX) systems, ultra-wideband (UWB) systems and UMTS Long Term Evolution (LTE) [8, 13].

An OFDM system works as follows: a binary data is mapped into a selected *M-ary* signal constellation. Afterward, a serial to parallel (S/P) conversion is applied to the resulting complex numbers. It is at this stage that known mapped pilot symbols

are appended into the OFDM signal. Then the inverse fast fourier transform (IFFT) operation is performed, and the CP is added between every block in order to avoid ISI. Finally, the transformed data is grouped again by a parallel to serial (P/S) conversion resulting into the OFDM transmitted signal [8].

The baseband modulated OFDM waveform, $s(t)$, can be expressed by N symbols being transmitted by different subcarriers, that is

$$s(t) = \sum_{k=0}^{N-1} S_k e^{j2\pi f_k t}, 0 \leq t \leq T_{symb}, \tag{2.4}$$

where S_k denotes the transmitted complex symbol at a minimum rate of $\frac{1}{T_s}$ and f_k is the k^{th} carrier frequency at which S_k symbol is transmitted. Note that T_s represents the symbol duration, so, the total OFDM block duration is given by NT_s.

One of the OFDM advantages is its low complexity which results of being easily implemented in the digital domain based on the DFT and IDFT, that can be efficiently computed by the fast fourier transform (FFT) and inverse FFT (IFFT) algorithms, respectively. In fact, applying the FFT/IFFT reduces significantly the complex multiplications from N^2 to $\frac{N}{2} log_2 N$. Also, these operations become faster and efficient if N is a power of two [5].

Applying this concept and admitting that each k^{th} carrier is separated by a spacing frequency of $\frac{1}{NT_s}$ (to avoid ICI), the digital OFDM signal can be expressed as [6]

$$s[n] = \sum_{k=0}^{N-1} S_k e^{\frac{j2\pi nk}{N}}, n = 0, ..., N-1. \tag{2.5}$$

Between the transmitter and receiver, the OFDM signal goes through a hostile wireless channel, being typically corrupted by additive white gaussian noise (AWGN), and subjected to fading due to multipath propagation effects. Therefore the received analog signal is converted to the digital domain, and then the synchronization tasks are executed, i.e., both carrier frequency and timing synchronization. After performing the S/P conversion the next steps are to demodulate the OFDM signal using the FFT operation and perform channel estimation and equalization, through the pilot symbols. Finally, another P/S conversion is executed and the complex received data are obtained through demapping by the same *M-ary* signal constellation, hence, recovering the original transmitted bit stream.

2.4.1 Drawbacks of OFDM modulation

Nevertheless, OFDM retains several disadvantages. This MC technique is extremely sensible to frequency and timing synchronization errors where any frequency offset, Δf, ruins the orthogonality between OFDM subcarriers, causing ICI.

Therefore, both the transmitter and receiver must retain the same frequency of reference. The main reason for frequency synchronization errors are caused by either the mismatched between the local oscillators (LO) from both ends of the transceiver system or relative motion between the transmitter and receiver, which in turn also causes Doppler spread [8].

The need of a Guard Interval (either a CP or ZP) comes with the cost in a loss of spectral efficiency. When the CP is implemented we typically call the system as CP-OFDM that has a total signal length of $N_{CP\_OFDM} = N_{CP} + N$. The term N_{CP} constitutes the CP size and must be higher than the channel delay spread in order to avoid ISI, Hence, we can typically say that OFDM suffers from a CP overhead that damages the system power efficiency [7].

An OFDM symbol, represented in (2.5), is windowed by a time domain rectangular window, $w[n]$, and can be denoted by

$$s[n] = \sum_{k=0}^{N-1} S_k w[n] e^{\frac{j2\pi kn}{N}}, n = 0, ..., N-1. \tag{2.6}$$

This window configuration is equivalent, in the frequency domain, to a *sinc* waveform. Therefore, the OFDM block embodies the superposition sum of N shifted *sinc* shaped spectrums, each centered at a different subcarrier frequency f_k. The main disadvantage of this windowing technique is its theoretical infinite bandwidth that causes a high out of band (OOB) emission. Hence, these lateral spectral side lobes can cause interference in the neighbour symbols spectrum, affecting the overall system spectral efficiency.

Another challenge that OFDM systems features is the non-constant envelope with high peaks, resulting in a high PAPR. The PAPR of a continuous-time signal, $x(t)$, is the ratio between the maximum signal's instantaneous power to its average power [6], that is,

$$PAPR = \frac{max|x(t)|^2}{E\left\{|x(t)|^2\right\}} \Leftrightarrow 10\log_{10}\left(\frac{max[x(t)x^*(t)]}{E[x(t)x^*(t)]}\right)[dB]. \tag{2.7}$$

Such high peaks will deliver signal excursions into the nonlinear region of operation of the transmitter's power amplifier, thereby leading to nonlinear distortions and spectral spreading. Also, the PAPR is affected proportionally with the increase of the numbers of OFDM subcarriers. Therefore, the power amplifiers must accommodate a large dynamic range to perform in the linear operation region, and be operated with some amount of back-off at amplifier's input which considerably decreases its efficiency [6, 15].

2.5 Hybrid Multicarrier Transmission Techniques

The OFDM high levels of radiation outside the channel band cause ICI, since the typical rectangular window applied exhibits a *sinc* wave spectrum that contains elevated lateral lobes.

To tackle this main OFDM's drawback, a hybrid transceiver system, denoted by BWB-OFDM [1, 2], was proposed. Its primary motivation is to achieve a more efficient spectral confinement while also continuing to guarantee the low complexity architecture of conventional OFDM schemes.

2.5.1 BWB-OFDM

A most efficient spectral confinement can be ensured by windowing each OFDM symbol in the time domain where this is cyclically extended and then multiplied by a square root raised cosine (SRRC) window [16] defined as

$$h_{SRRC}[n] = \begin{cases} 1 & ,|n| \leq \frac{N}{2}(1-\beta) \\ cos(\frac{\pi}{4\beta}[\frac{2n}{N} - (1-\beta)]) & ,\frac{N}{2}(1-\beta) \leq |n| \leq \frac{N}{2}(1+\beta). \\ 0 & ,|n| \geq \frac{N}{2}(1+\beta) \end{cases} \tag{2.8}$$

where β is the window roll-off, with $\beta = 0$ corresponding to the rectangular window. The previously defined SRRC window guarantees an attenuation of the secondary lobes, the higher the value of β, therefore allowing a more spectral efficiency.

It is possible to see the OFDM power spectral density (PSD) differences between the two windowing techniques in the following Figure:

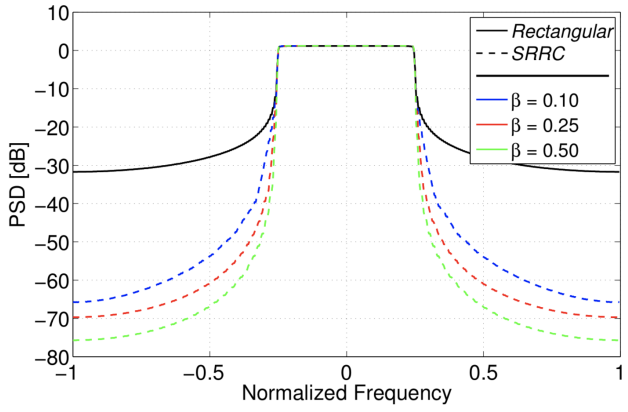

Figure 2.1: Signal PSD of windowed OFDM with a time-domain SRRC window as a function of the roll-off [1, 2]. (Note: the frequency axis is normalized by $\frac{2}{T_s}$.)

The building process of a BWB-OFDM symbol, presented in Figure 2.2, consists into packing together a set of N_s conventional OFDM symbols, $\mathbf{s}_{n,i}$ with $i =$

$1,...,N_s$, wherein in each one of them is applied the previously described windowing operation, i.e, a cyclic extension and a Hadamard multiplication in the time domain by a SRRC window. Mathematically, the windowing process can be represented by the following expression

$$\mathbf{s}_{\mathrm{w,i}} = [\mathbf{s}_{\mathrm{n,i}}|\mathbf{s}_{\mathrm{n,i}}]_{(1\times 2\mathrm{N})} \odot \mathbf{h}_{\mathrm{SRRC}_{(1\times 2\mathrm{N})}}. \tag{2.9}$$

Additionally, in the BWB-OFDM technique, the CP between each OFDM symbol is discarded, and only one guard interval, zero-pad (ZP), is applied to the set of N_s consecutive OFDM symbols, $\mathbf{s}_{\mathrm{w,i}}$, with the BWB-OFDM symbol being defined as

$$\mathbf{x}_n = [\mathbf{s}_{\mathrm{B}}|0_{(1\times \mathrm{N_{zp}})}]_{(1\times \mathrm{N_x})}, \tag{2.10}$$

with

$$\mathbf{s}_{\mathrm{B}} = [\mathbf{s}_{w,1}|\mathbf{s}_{w,2}|...|\mathbf{s}_{w,N_s}]_{(1\times \mathrm{N_B})}, \tag{2.11}$$

where $N_B = N_s \times N(1+\beta)$.

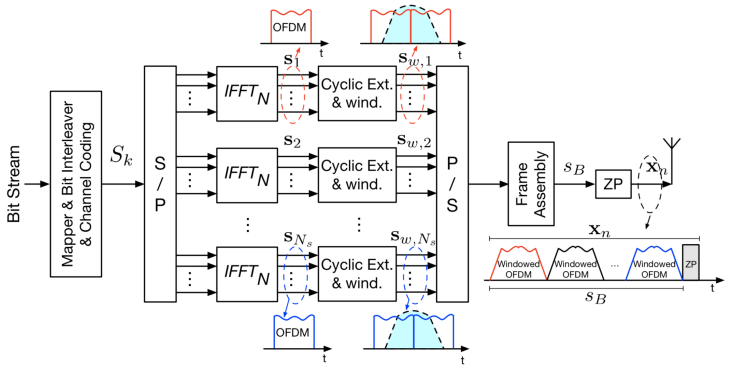

Figure 2.2: BWB-OFDM transmitter scheme model [1, 2].

The BWB-OFDM block unformatting process, illustrated in figure 2.3, begins with a frequency domain equalization (FDE) treating the received signal, y_n, as a single carrier block. After this process, the estimated signal $\hat{X}_k$ is converted to the time domain, and the guard interval (ZP) is removed. Then, the matched filtering is performed, where in order to avoid ICI, the SRRC window must be identical in the different stages of the transceiver scheme. Therefore, the estimated $\hat{\mathbf{s}}_{\mathrm{w,i}}$ symbols are expressed by

$$\hat{\mathbf{s}}_{\mathrm{w,i}} = \hat{\mathbf{x}}_{\mathrm{n,i}(1\times 2\mathrm{N})} \odot \mathbf{h}_{\mathrm{SRRC}(1\times 2\mathrm{N})}. \tag{2.12}$$

Finally, the symbols are converted to the frequency domain, employing the DFT operation, i.e., $\hat{\mathbf{S}}_{w,i} = DFT\{\hat{\mathbf{s}}_{w,i}\}$, and then demodulation, channel decoding, demapping, and bit-deinterleaving operations are performed.

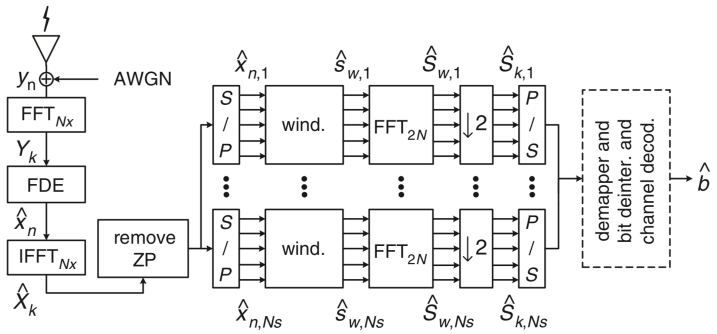

Figure 2.3: BWB-OFDM receiver scheme model [1].

The use of the windowing technique and a sole ZP per group of N_s OFDM block allow us to conclude that the BWB-OFDM allows a more efficient spectral confinement while keeping high data transmission rates and the orthogonality between OFDM subcarriers. However, as represented in figure 2.4, these systems feature the same drawbacks of the OFDM scheme regarding deep fade regions in a frequency selective channel, namely when a set of subcarriers lay inside a deep fading region, causing in a complete loss of information.

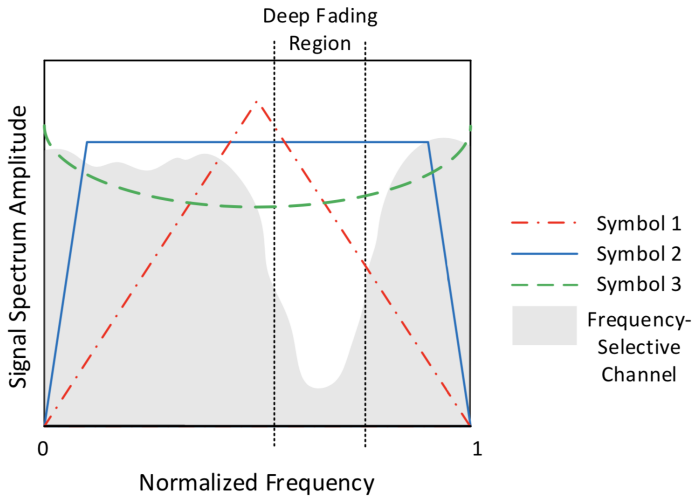

Figure 2.4: Illustration of a BWB-OFDM signal spectrum composed by 3 OFDM symbols [2].

Hence, the recovering process of the transmitted signal is too complex, and consequently, the overall system performance suffers from degradation.

For that purpose, a new burst technique based on BWB-OFDM, denominated as TIBWB-OFDM, was developed to deal against the dispersive channel effects on transmitted data.

2.5.2 TIBWB-OFDM

The TIBWB-OFDM [2, 3] is also considered as a hybrid modulation technique since the receiver is practically identical to the BWB-OFDM receiver in terms of equalization of the received signal. As shown in Figure 2.5, the most straightforward approach to preserve all data destroyed by the deep fading effect is to replicate the information over the entire channel bandwidth assigned.

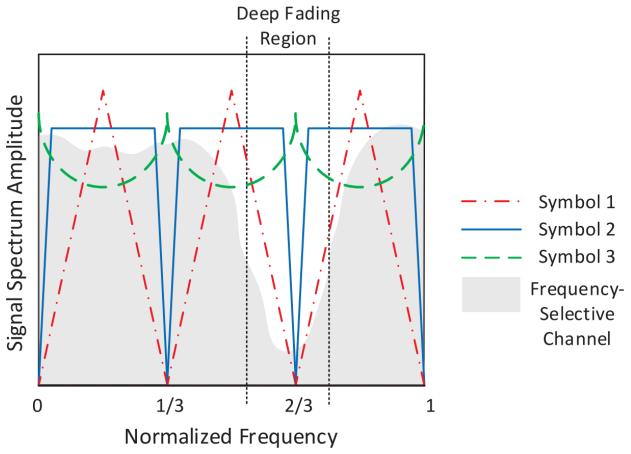

Figure 2.5: Illustration of a TIBWB-OFDM signal spectrum composed by 3 OFDM symbols [2].

The described procedure resembles to perform a time-interleave operation between the samples of the corresponding BWB-OFDM symbol.

Like the BWB-OFDM modulation, the TIBWB-OFDM transmitter scheme, represented in Figure 2.6, is composed by a set of N_s OFDM symbols, $\mathbf{s}_{n,i}$, which suffer a time-domain windowing according to (2.12) and are packed together as in (2.11).

After the time domain juxtaposition of the windowed OFDM symbols it is performed the interleaving operation with the resulting interleaved block vector being given by:

$$\mathbf{s}_\pi = \mathbf{s}_\mathbf{w}\Pi^{(N_s)}, \tag{2.13}$$

where $\Pi^{(N_s)}$ represents the time-interleave matrix with period N_s and size $[N_{symb} \times N_{symb}]$. This is a matrix where the $\mathbf{c}$ column has a single $\mathbf{1}$ at line,

$$\left\lfloor \frac{c}{N_s} \right\rfloor + (cN_{\text{symb}} \mod N_{\text{symb}}N_s), \tag{2.14}$$

being 0 otherwise.

Finally, a ZP vector is added at the end of each TIBWB-OFDM block. In order to avoid any ISI, the null vector length, N_{zp}, must be greater than the channel prop-

agation delay. Therefore, the obtained transmitted mega-block, $\mathbf{x}_n$, is represented as:

$$\mathbf{x}_{\mathrm{n}} = [\mathbf{s}_{\pi} | 0_{(1\times N_{zp})}]_{1\times N_x}, \tag{2.15}$$

with vector $\mathbf{x}$ length of $N_x = N_{zp} + N_s \times N_{Symb}$ [4].

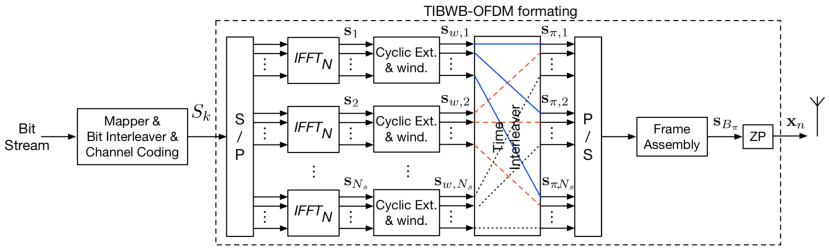

Figure 2.6: Transmitter scheme of TIBWB-OFDM modulation [3].

The TIBWB-OFDM receiver key task is to perform equalization and unformat the received mega-block. The latter operation is established by executing the opposite of the transmitter scheme. That is, perform the block time-deinterleaving, matched filtering, demodulation, and channel decoding. The receiver design is represented in Figure 2.7.

The received signal is converted to the frequency domain through an N_x sized DFT operation, resulting in $Y_k = DFT\{y_n\}$, with $k = 0,1,...,N_x - 1$. Assuming that the use of ZP eliminates total ISI, linear FDE can be executed by means of several equalization algorithms. These algorithms are explored with more detail in Section 3.2. After equalization, the frequency domain estimated signal, $\hat{X}_k$, with $k = 0,1,...,N_x - 1$, is converted by a N_x sized IFFT to the time domain and the guard interval (ZP) is removed. The equalized TIBWB-OFDM block is then and, after, it is splitted into its component windowed OFDM blocks. Each of these is matched filtered by employing the same SRRC window used upon transmission. For that, it is important to add a number of zeros so that the total length is equal to $2N$ [2]. The windowing process, is similar to the one in 2.12 and follows

$$\hat{\mathbf{s}}_{\mathrm{w,i}} = \hat{\mathbf{x}}_{\mathrm{w,i}(1\times 2\mathrm{N})} \odot \mathbf{h}_{\mathrm{SRRC}(1\times 2\mathrm{N})}. \tag{2.16}$$

To obtain an estimation of the original transmitted symbol, $\mathbf{S}_k$, the estimated previous sub-symbols, $\hat{\mathbf{s}}_{w,i}$, are converted back to the frequency domain by a 2N size FFT and downsampled by 2, resulting in

$$\hat{\mathbf{S}}_{\mathrm{k,i}}[n] = \hat{\mathbf{S}}_{\mathrm{w,i}}[\mathbf{2n}]_{(1\times 2N)}. \tag{2.17}$$

At last, it is applied the bit-deinterleaving, de-mapping and channel decoding operations on each $\hat{S}_{k,i}$ symbols to obtain the final estimated sequence, denoted as $\hat{b}$

in Figure 2.7. As previously stated, the receiver executes linear frequency domain

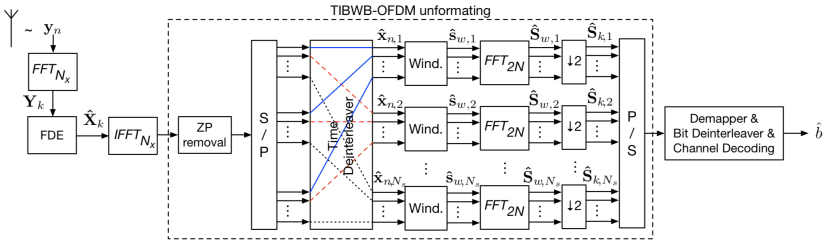

Figure 2.7: Receiver scheme of TIBWB-OFDM modulation [3].

equalizers, where although feature low complexity, can perform with a satisfactory performance. However, the performance is far from the matched filter bound (MFB) so the alternative approach arrives by adopting nonlinear schemes such as decision feedback equalizers in the original TIBWB-OFDM modulation scheme [17]. A promising equalization scheme, capable of performing close to the MFB in rich multipath propagation channels, is the IB-DFE [17, 18]. In the following Section this concept is explored to perform the equalization operation.

2.5.3 TIBWB-OFDM with IB-DFE receiver

The IB-DFE equalizer, depicted in Figure 2.8, is particularly suited for block-based single-carrier type transmissions. This scheme can deal with ISI or inter-block interference (IBI), due to the multipath time-dispersive [3] effects, by means of two important filter: the **feedforward filter (FF filter)** ($\mathbf{F}_k^l$) and the **feedback filter (FB filter)** ($\mathbf{B}_k^l$). The first filter acts like a conventional FDE, where it aims to decrease the precursors created by the wireless channel. The second one attempts to cancel the remaining ISI or IBI through information from previous precursors.

So, the equalizer processes the received signal, $\mathbf{Y}_k$, where performs at each $\boldsymbol{l}$ iteration an equalized TIBWB-OFDM symbol, i.e., $\tilde{\mathbf{X}}_k(l) = \{\tilde{X}_k(l) : k = 0, ..., N_x - 1\}$ with

$$\tilde{X}_k^{(l)} = F_k^{(l)} Y_k - B_k^{(l)} \hat{X}_k^{(l-1)}, \tag{2.18}$$

where $\hat{\mathbf{X}}_k^{(l-1)}$ denotes the frequency domain signal estimated at the previous iteration, by either performing a *hard* or *soft* FB filter decision of $\hat{\mathbf{x}}_n^{(l-1)}$ [3].

The optimal FF filter and FB filter filter coefficients are, respectively, given by

$$F_k^l = \frac{\kappa H_k^*}{\frac{1}{\gamma} + \left(1 - (\rho_{blk}^{l-1})^2\right) |H_k|^2}, \tag{2.19}$$

and

$$B_k^l = \rho_{blk}^{l-1} \left(F_k^l H_k - 1\right), \tag{2.20}$$

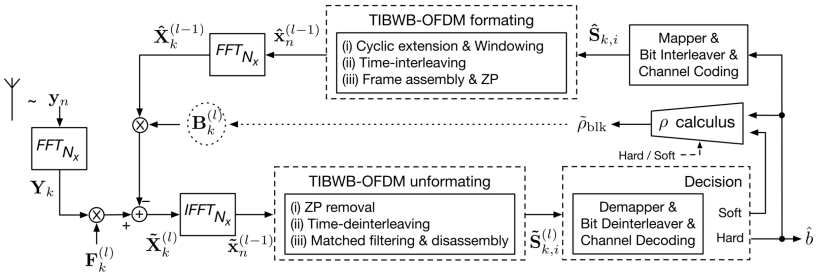

Figure 2.8: TIBWB-OFDM modulation scheme with IB-DFE receiver [3].

where κ denotes a normalized constant chosen to guarantee that $\frac{1}{N}\sum_{k=0}^{N-1} F_k^l H_k = 1$ and γ is the signal-to-noise ratio (SNR). Also, ρ_{blk} represents the correlation factor and is the key parameter for a reliable IB-DFE operation and a accurate system performance [19]. It can be represented as

$$\rho_{blk}^{l-1} = \underbrace{\frac{E\left[\hat{x}_n^{l-1} x_n\right]}{E\left[|x_n|^2\right]}}_{\text{time domain}} = \overbrace{\frac{E\left[\hat{X}_k^{l-1} X_k\right]}{E\left[|X_k|^2\right]}}^{\text{frequency domain}} \tag{2.21}$$

A typical good approximation of (2.21) can be computed by replacing the transmitted TIBWB-OFDM signal term with the output FF filter signal, $\tilde{x}_n^{l-1}$, resulting in

$$\rho_{blk}^{l-1} = \frac{E\left[\hat{x}_n^{l-1} \tilde{x}_n^{l-1}\right]}{E\left[|\tilde{x}_n^{l-1}|^2\right]} \tag{2.22}$$

It is possible to conclude, that in the first IB-DFE iteration, the ρ_{blk} factor is zero. So, it can be classified as a simple linear equalizer since the FB filter has also null coefficients and the FF filter is similar to the minimum mean square error (MMSE) equalizer, explained with more detailed in Section 3.2.

In terms of the IB-DFE remains explaining how the device decision works. Its purpose is to provide the best block estimation in order to guarantee a good measure of the block reliability and is divided in two categories: the *hard* or *soft* estimation [3].

The most simple method is to perform a *hard* computation. It is based on the minimum distance criteria, where the decision belongs to the closer distance between the estimated symbol and the constellation symbol. However, under a *soft* decision computation, the IB-DFE accuracy is widely improved and hence the overall system performance since each bit-wise decision is computed by a log-likehood probability algorithm instead of taking always a "fixed" decision.

It is logic to think that the decision device accuracy levels in data estimation affect the correlation factor and, therefore, the overall system performance, so it is an important topic to explore. Also, the addition of channel coding in the IB-DFE loop can improve even more the equalization process [3].

2.5.3.A IB-DFE receiver with *soft* device decisions

Improving the IB-DFE performance is achieved by implementing a symbol by symbol estimation, $\tilde{S}_{k_i}$, instead of a *blockwise average*. Consider, as an example, the scenario where each OFDM subcarrier is modulated using a quadrature phase shift keying (QPSK) constellation with Gray mapping, that maps each x of bits (b_0, b_1) to the constellation symbol, $S_{k_i} = \beta_0 + j\beta_1 = \pm 1 \pm j$, with $\beta_i = (-1)^{b_i}$ being the polar representation of bit b_i. So the log-likelihood ratio (LLR) information, referenced to the received $\tilde{S}_{k_i}$ symbol, is given by [3]

$$\lambda_{k_i}^{b_0} = \log\left(\frac{Prob\left\{b_0 = 0|\tilde{S}_{k_i}\right\}}{Prob\{b_0 = 1|\tilde{S}_{k_i}\}}\right) = \frac{4\Re\left\{\tilde{S}_{k_i}\right\}}{\sigma_\eta^2}, \tag{2.23}$$

and

$$\lambda_{k_i}^{b_1} = \log\left(\frac{Prob\left\{b_1 = 0|\tilde{S}_{k_i}\right\}}{Prob\left\{b_1 = 1|\tilde{S}_{k_i}\right\}}\right) = \frac{4\Im\left\{\tilde{S}_{k_i}\right\}}{\sigma_\eta^2}, \tag{2.24}$$

where σ_η^2 constitutes the variance of the complex noise plus residual interference at the FF filter output. The average bit values resulting from *soft* demodulation, caused by the LLR values, are represented by

$$\bar{\beta}_0 = Prob\{b_0 = 0\} - Prob\{b_0 = 1\} = tanh\left(\frac{\lambda_{k_i}^{b_0}}{2}\right), \tag{2.25}$$

and

$$\bar{\beta}_1 = Prob\{b_1 = 0\} - Prob\{b_1 = 1\} = tanh\left(\frac{\lambda_{k_i}^{b_1}}{2}\right), \tag{2.26}$$

where the reliability of the average bits of these are, respectively, given by

$$\rho_{k_i}^{b_0} = |\bar{\beta}_0| = tanh\left(\frac{|\lambda_{k_i}^{b_0}|}{2}\right), \tag{2.27}$$

and

$$\rho_{k_i}^{b_1} = |\bar{\beta}_1| = tanh\left(\frac{|\lambda_{k_i}^{b_1}|}{2}\right). \tag{2.28}$$

Therefore, the block-wise soft reliability factor, $\tilde{\rho}_{blk}$, is computed as

$$\tilde{\rho}_{blk} = \frac{1}{2}\sum_{i=1}^{N_s}\sum_{k=0}^{N-1}\left(\rho_{k_i}^{b_0} + \rho_{k_i}^{b_1}\right). \tag{2.29}$$

The computation of σ_η^2, to use in (2.23) and (2.24), is a complex process for the TIBWB-OFDM scenario. In this case, the variance term is estimated in the first IB-DFE iteration, by performing a kind of average on the signal to noise ratio, γ, along the signal bandwidth [3]. Therefore, σ_η^2 can be computed as

$$\sigma_\eta^2 = \frac{\varepsilon_s}{N_x} \sum_{k=0}^{N_x-1} \frac{1}{1+\gamma|H_k|^2}, \tag{2.30}$$

where ε_s is the power transmitted per modulated symbol, which in the QPSK modulation scenario, $\varepsilon_s = 2$.

2.5.4 TIBWB-OFDM with WTO

As previously explained, although all the advantages presented in the conventional TIBWB-OFDM modulation, relatively to the traditional CP-OFDM scheme, there is still some limitation imposed by the size of the window roll-off. Increasing the β factor causes better spectral confinement. However, the TIBWB-OFDM block length, equal to $N_{block} = N_s \times N(1+\beta)$, also increases. This causes the symbol transmission rate to decrease and therefore limits the spectral efficiency gains [4]. In [4], it is addressed the overall average power reduction due to the windowing operation, which increases the transmitted signal PAPR of the TIBWB-OFDM symbol.

To address both these problems an alternative TIBWB-OFDM packing method called TIBWB-OFDM with windowing time overlapping (TIBWB-OFDM WTO) [4], was proposed based on the premise of allowing partial overlapping windowing symbols. As shown in Figure 2.9, this packing method follows the SRRC windowing procedure, previously addressed in (2.2), and precedes the time-interleaving operation.

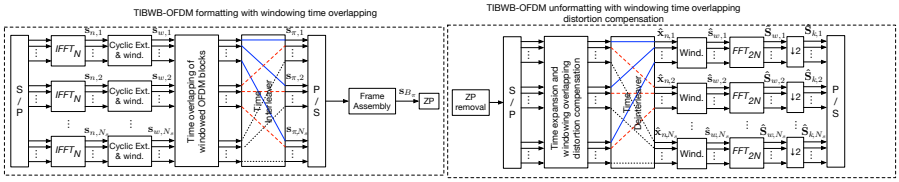

Figure 2.9: TIBWB-OFDM WTO modulation transceiver scheme [4].

Instead of juxtaposing the windowed OFDM symbols to each other, as in (2.11), the new TIBWB-OFDM with WTO partial overlappes the tails of the windowed OFDM symbols. Mathematically, the new packing method can be represented as

$$s_{wo}[n] = \sum_{i=1}^{N_s} s_{w_i}[n-(i-1)N_l] \quad \text{and } N \leq N_l \leq N_{\text{symb}}, \tag{2.31}$$

where N_l represents each block first overlapped sample. (2.31) can also be expressed as a vector shape matrix by

$$\mathbf{s_{wo}} = \mathbf{s_w}\mathbf{G_o}, \tag{2.32}$$

where $\mathbf{G_o}$ is a rectangular matrix that group OFDM component blocks with overlapping. A more clarifying matrix structure of $\mathbf{G_o}$ is shown in Figure 2.10. Note that $\mathbb{I}_{N_{\text{symb}}}$ represents the N_{symb} by N_{symb} dimensional identity matrix.

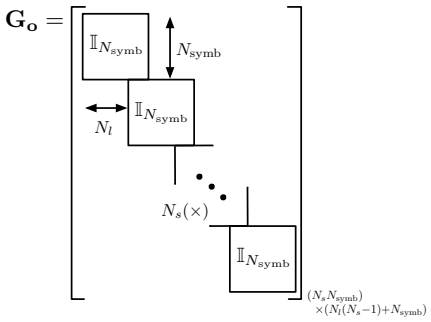

Figure 2.10: Schematic of the overlapping matrix structure, $\mathbf{G_o}$ [4].

The remaining construction phases of the transmitted block are identical to the conventional TIBWB-OFDM scheme with $\mathbf{s_{wo}}$ replacing the BWB-OFDM block vector, , $\mathbf{s_w}$, as in (2.13).

Figure 2.11 illustrates an intuitive manner of this new packing and the relation between the mega-block length and N_l. Once the N_s symbols that format the BWB-OFDM block are now either full or partial overlapped, it is inevitable to avoid interference between them (N_{os} is refereed to the dynamic term that represents the number of overlapped samples and is given by $N_{os} = N_{symb} - N_l$) [4]. Hence, the receiver will have the task of applying interference cancellation methods to recover the windowed overlapped received signal.

The new waveform overall total length is $N_{OB} = N_l(N_s - 1) + N_{symb}$ (with ZP not included) where:

(i) if $\boldsymbol{N}_l = \boldsymbol{N} \rightarrow N_{OB} = N(N_s - 1) + N(1 + \beta) = N(N_s + \beta)$

(ii) if $\boldsymbol{N}_l = \boldsymbol{N}(1 + \beta) \rightarrow N_{OB} = N(1 + \beta)(N_s - 1) + N(1 + \beta) = N_s N(1 + \beta) \Leftrightarrow$
$\Leftrightarrow N_{OB} = \boldsymbol{N}_{block}$

This means that (i) describes the scenario where the tails from windowed OFDM symbols are fully overlapped. Since $\beta < 1$, the previous scenario length, $N(N_s + \beta)$, is approximately equal to $N \times N_s$ which is the OFDM symbol total length with rectangular windowing. Hence, it is said that there is no temporal extension comparing

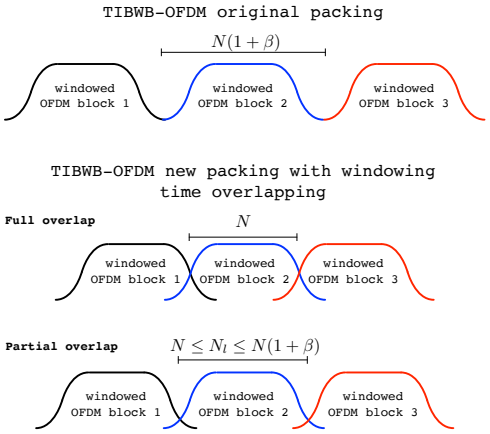

Figure 2.11: Waveform packing technique differences between the conventional TIBWB-OFDM and TIBWB-OFDM WTO [4].

to the OFDM waveform. The scenario (ii) represents the opposite limiting case corresponding to the original TIBWB-OFDM packing.

In conclusion, the TIBWB-OFDM WTO technique is capable of achieve an even better spectrum confinement with high spectral efficiency and data rates [4].

The WTO receiver scheme must perform two equalization steps: first a FDE and then a TDE to eliminate the undesired sub-block interference. As Figure 2.12 shows, it is applied a linear FDE with successive forward and backward cancellation. This method is possible since the original BWB-OFDM block is cyclically

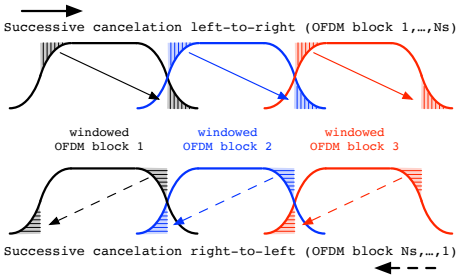

Figure 2.12: Equalization interference cancellation algorithm concept [4].

extended before the applying the SRRC window. Either applying ZF or MMSE equalization schemes [4], studied in the next Section, the main principle for retrieving the correct information, is to use the first received symbol, that as no interference, and then estimating the interference caused by the head of the second symbol, and so on. The inverse operation, is obtained by the same logic.

3

Channel Estimation, Equalization and Synchronization Techniques

Contents

This Section will introduce channel estimation, equalization and signal recovery concepts, which are essential for wireless communications among multiple devices. It begins by addressing synchronization methods as an important step that must be performed to achieve a reliable data detection and thus obtain a high system performance. Since the wireless channel affects the transmitted signal, the receiver must be designed in order to perform frame detection, timing recovery and carrier frequency correction. Only afterwards, it is possible to move into the equalization, channel estimation and decoding tasks.

3.1 Synchronization

The literature on the synchronization for OFDM-based systems [5,6,9] falls into the following criteria:

1. sampling clock synchronization: the sampling clock period at the receiver is slightly different from the corresponding sampling period at the transmitter resulting in a sampling clock offset (SCO), Δ_{clock}, that implies sampling the received waveform at an interval of $(1+\Delta_{clock})T_s$, instead of the ideal T_s, causing ICI in the overall system performance;

2. timing synchronization: trying to detect the beginning, T_d, of each received symbol/frame to identify the exact position of the frame beginning. If not properly located, then the timing window is incorrectly selected, leading to ISI;

3. frequency synchronization: attempting to cancel the frequency error between the transceiver that causes in a rotation at a frequency of δ_f of the received complex baseband signal, also called as carrier frequency offset (CFO), which results in a degradation of orthogonal property among subcarriers. Therefore, frequency synchronization is essential to restore the carrier orthogonality properties and consequently to avoid ICI.

In Figure 3.1 is depicted all the described offsets effects that synchronization algorithms must eliminate. Timing errors delay, $n_\Delta T_d$, occurs because of most communications systems' inability to guarantee the same time reference signal and the propagation time between both transceptors devices [20].

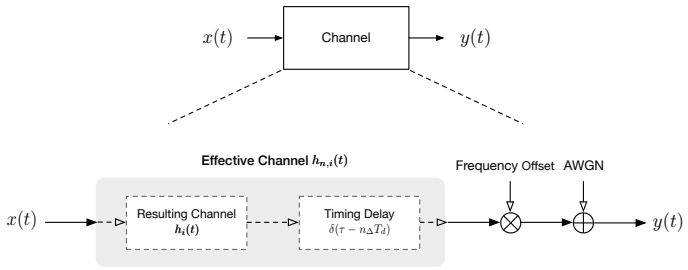

Figure 3.1: Wireless channel model containing several interference that signals are subjected.

Therefore, the previous effective channel notation (2.3) is now represented as

$$h_\Delta(\tau;t) = h(\tau;t) * \delta(\tau - n_\Delta T_d). \tag{3.1}$$

The effects of a slight n_Δ shift can drastically affect the system performance. Since the receiver channel estimation follows a specific window to produce an unbiased and accurate signal estimation, if some of these samples are undesirably shifted, it is impossible to achieve a good BER relation [20].

3.1.1 Symbol Offset Synchronization and Frame Detection

In order to eliminate this mismatch and perform timing estimation, it is important to first detect the presence of data, by a measuring the signal received power, and then estimate the beginning of the preambles sequences. Therefore, the principle of frame detection [21] is based on the use of markers, which are typically known at the receiver and have proprieties that facilitate the frame and channel computation, if jointly estimated. The frame beginning position is estimated by searching for periodic structure within the signal, i.e., applying correlation signal techniques between the received frame and known markers [22]. Therefore, the use of cross-correlation is a possible and reliable method to provide an appropriate frame detection. It combines the transmitted data, y, with the preamble, p_n. This step can be performed as shown in (3.2) which is identical to perform the convolution of the inverse conjugate preamble samples with the received signal

$$\mathrm{C}_{y,p_n}(l) = \sum_m y^*(m) p_n(m+l). \tag{3.2}$$

Depending on the chosen preamble sequence and their proprieties, it is expected that when $y \approx p_n$, at least a high peak is produced. When correlating a sequence with itself, the highest correlation peak, C_{max}, appears at index L_p and is given by

$$\mathrm{C}_{max} = \sum |p_n|^2. \tag{3.3}$$

where the total correlation length is equal to $2L_p - 1$.

When the frame's estimated starting point is obtained, it is important to decide if the marked position is indeed the beginning of the frame or not, i.e., define a detection probability as

$$\mathscr{H}_0 : \text{Signal absence} \quad \text{and} \quad \mathscr{H}_1 : \text{Signal detected}, \tag{3.4}$$

which can be also represented as

$$\mathscr{H}_0 : y_n = \eta \quad \text{and} \quad \mathscr{H}_1 : y_n = x_n + \eta, \tag{3.5}$$

where for the absence hypothesis, the received signal is composed only by the noise component, η, and, on the other hand, the detected hypothesis is the superposition between the noise, and transmitted signal blocks, x_n. Based on C_{max} and the noise distribution, it is important to define a threshold decision rule that affects the symbol detection in order to maximize the success frame detection probability (P_D) and reduces situations of either false alarm (P_F) or missed frame detection (P_M). Mathematically these probabilities definitions can be expressed as

$$P_M = P\{\text{Select } \mathscr{H}_1 | \mathscr{H}_0\} \text{ and } P_F = P\{\text{Select } \mathscr{H}_0 | \mathscr{H}_1\}, \tag{3.6}$$

where the probability of detection, P_D, is derived as follows

$$P_D = 1 - P_M = P\{Select \mathscr{H}_1 | \mathscr{H}_1\}. \tag{3.7}$$

A binary decision is made based on this threshold rule device, where $\delta_{decision} = \{0,1\}$, and an intercession region is marked.

This frame detection procedure has the advantage of being computationally low and can be adopted as a coarse synchronization step in the receiver design. It is also possible to perform a fine timing synchronization stage based on digital filtering with interpolated data at a four times higher rate than the original data rate to provide an even more accurate timing compensation. Actually, the filtered up-sampled data provides additional high-resolution samples causing the resolution of the correlation algorithm to increase [23].

3.1.2 Frequency Offset Synchronization

A slight small frequency mismatch between the transmitter and receiver's LO is sufficient to impact the overall system performance. The difference, $\delta_f = f_{Tx_{LO}} - f_{x_{LO}}$, is refereed as the CFO, and reflects in a rotation of the constellation obtained,

i.e., a signal phase shift of $2\pi\delta ft$. Then, the received baseband signal, $y(t)$, in each k_{th} subcarrier, considering the transmission [21],

$$y(t) = x(t)e^{j(\overbrace{2\pi\delta_f}^{w_0}t+\theta)} + n(t), \tag{3.8}$$

where $n(t)$ denotes the AWGN samples.

As illustrated in Figure 3.2, the impact of a frequency error can be seen as an error in the frequency instants, where the received signal is sampled during demodulation by the FFT. With the appearance of these frequency deviations, ICI occurs

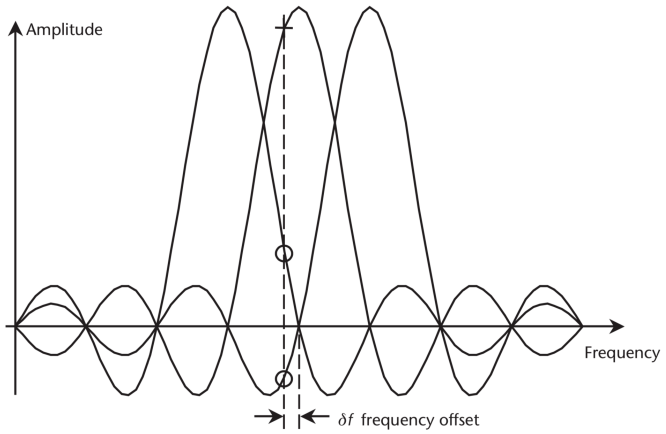

Figure 3.2: Example of an individual superimposed spectrum of an OFDM block affected by a subcarrier frequency mismatch [5].

due to loss of orthogonality among subcarriers. Nevertheless, if the frequency offset is a multiple integer of the subcarriers spacing the total mismatch between subcarrier remains $\Delta f = \frac{1}{T_{symb}}$, and in this case, ICI is avoided. However, the signal is shifted by a factor of $k \times \frac{1}{T_{symb}}$ leading to a wrong position of the received spectrum which increases the system BER [24].

Typically, the CFO is compensated by performing two-stage frequency synchronization: first, a coarse and then a fine frequency correction. Like timing synchronization, the frequency correction is typically based on pilots or cyclic prefix techniques which allow to estimate the signal phase rotations. Pilot tones based algorithms can be easily used to detect the frequency mismatch received sequence, visible by the phase rotation speed, and shifted back to the right position.

Similar to timing synchronization, some methods also propose to adopt the correlation proprieties of identical pilot symbols to estimate the carrier phase offset [25].

Although its relevance, in this work, it is assumed that the receiver can handle the CFO and the research priority is made on the development of joint frame synchronization and channel estimation for the TIBWB-OFDM modulation technique.

3.1.3 Zaddoff-Chu Sequences

An essential part for achieving a reliable frequency and timing recovery is the choice of optimum preamble sequences. In the LTE communication schemes, as part of the system acquisition process, two preamble sequences defined as primary synchronization signal (PSS) and secondary synchronization signal (SSS) are used in the downlink process [26]. Although these SSS sequences are based on maximum length sequences, also known as M-sequences, the PSS is composed by ZC sequences [27], a complex-valued mathematical sequence with good properties to use in synchronization techniques for accurate timing estimation [28].

Mathematically, the sequence of odd-length period N_{ZC} is generated as [26],

$$zc_n[q] = e^{\frac{-j\pi nq(q+1)}{N_{ZC}}}, \quad q = 0,1,...,N_{ZC}-1, \tag{3.9}$$

where n is the root index and $n \in \{1,...,N_{ZC}-1\}$.

As referred, ZC sequences exhibit some fundamental proprieties that aid the receiver in the synchronization task [26, 29]:

(i) ZC sequences have a constant amplitude, i.e, the I/Q representation of these sequences is a perfect circle which, on the other hand, limits the PAPR;

(ii) ZC sequences have, in theory, "perfect" cyclic auto-correlation, i.e. the correlation with its circularly shifted version is zero at samples different from N_{ZC} and non-zero only at one instant which corresponds to the N_{ZC} sample. The zero auto-correlation ZC property can be formulated by (3.2), resulting in

$$\mathrm{C}_{zc,zc}[l] = \sum_m zc^*[l]zc[q+l] = P_{zc}[l], \tag{3.10}$$

where P_{zc} corresponds to the auto-correlation peak positioned in the delayed l sample. This is an important feature for wireless communications enabling misaligned ZC sequences to correlate between themselves. Hence, it is possible to generate multiple orthogonal sequences just by shifting the ZC sequence.

Sequences that combine the previous two proprieties are designated as constant amplitude zero auto correlation (CAZAC) sequences [29].

(iii) if we guarantee the Zadoff Chu sequence length N_{ZC} to be a prime number, then, in theory, the cross-correlation of these two sequences is $1/\sqrt{N_{ZC}}$.

A crucial application of ZC sequence is for time synchronization due to there CAZAC properties. Therefore the receiver by analysing the sequence correlation peak inside a timing slot can easily identify the transmitted frame beginning [30].

However, ZC sequences exhibit difficulties separating the frequency offset, resulting in additional time-domain correlation peaks caused by the fading channel delay. Furthermore, the sequence correct correlation peak amplitude is attenuated at high Doppler frequencies, which can lead to false detect or miss the frame beginning from the several time delay correlation peaks, causing to miss calculate the channel total delay and consequently decreasing the overall system performance [28].

3.2 Equalization

As referred, TIBWB-OFDM is an hybrid modulation technique, where the signal upon reception can be seen as a block-based SC transmission type and the equalization task processed in the frequency domain [2, 19]. When it comes to the FDE, this has several advantages over time-domain equalization (TDE) in outdoor high-mobility propagation environments and for channels with severe delay spreads, since the receiver complexity can be kept low [8]. In channels whose impulse responses remain constant within one transmitted symbol period, the received signal, Y_k, at each subcarrier $k = 0, ..., N-1$ can be expressed as

$$Y_k = H_k X_k + N_k, \tag{3.11}$$

where H_k represents the channel frequency response (CFR). By employing linear FDE the estimated signal is given by

$$\hat{X}_k = F_k Y_k \tag{3.12}$$

where F_k is the frequency response of the FeedForward equalization filter.

The two most popular linear equalization schemes are the zero-forcing (ZF) equalizer and the minimum mean square error (MMSE) equalizer. The zero forcing (ZF) equalizer simply uses the inverse of the CFR, i.e,

$$F_k = \frac{H_k^*}{|H_k|^2} = \frac{1}{H_k}. \tag{3.13}$$

By replacing in (3.12) the received signal is given by

$$\hat{X}_k = \frac{H_k X_k}{H_k} + \frac{N_k}{H_k} = X_k + \frac{N_k}{H_k}. \tag{3.14}$$

Although it's computational simplicity, this equalization technique results in noise enhancement caused on the term $\frac{N_k}{H_k}$ especially in the carriers that suffer deep fading.

In the case of an MMSE receiver, which tries to minimize $E\{|\hat{X}_k - X_k|^2\}$, takes the SNR component, γ, into account. Therefore the equalization weight on the subcarrier k is given as

$$F_k = \frac{H_k^*}{|H_k|^2 + \frac{1}{\gamma}}. \tag{3.15}$$

This equalizer has the advantage that the minimizes the noise enhancement problem in low SNR cases is gone although it does not a perfect inversion of the channel. Also, when the SNR is high enough, it is clear that the MMSE equalizer approaches the zero forcing equalizer [6]. Therefore, replacing the previous statement in (3.11) the estimated signal can be expressed as:

$$\hat{X}_k = \frac{H_k^* H_k X_k}{|H_k|^2 + \frac{1}{\gamma}} + \frac{N_k H_k^*}{|H_k|^2 + \frac{1}{\gamma}} = \frac{|H_k|^2 X_k}{|H_k|^2 + \frac{1}{\gamma}} + \frac{N_k H_k^*}{|H_k|^2 + \frac{1}{\gamma}}. \tag{3.16}$$

3.3 Channel Estimation

Another challenging obstacle in communications systems is the demanded necessity for the receiver to obtain instantaneous CSI, which is not an easy task due to time variance and frequency selectivity of wireless channels.

Therefore, pilots are carefully chosen depending on the maximum length of CIR and with the objective of minimizing the channel estimation error and the overall BER. They also need to be projected in order to maximize channel capacity by optimizing the pilot sequence length and distribution [31]. Channel estimation techniques can be classified into two categories [6, 32]:

(i) non-data-aided, where the CSI is obtained without the use of reference training signals, i.e., based on the statistics of the received signals sequences;

(ii) data-aided, which require added information, i.e., reference training signals that are included in the transmitted frame.

Although non-data-aided techniques do not require reference signals, a large number of data must be collected in order to obtain reliable estimation channel samples. Hence, data-aided techniques, although requiring an additional frame overhead on the transmitted data, that causes a decrease in the spectral efficiency, can provide better performance, especially on fast changing channel conditions.

According to (3.11) the received signal can be written in vector format as

$$\mathbf{Y} = diag(\mathbf{X})\mathbf{H} + \mathbf{N}, \tag{3.17}$$

where $\mathbf{X} = [X_1, ..., X_N]^T$, $\mathbf{H} = [H_1, ..., H_N]^T$ and $\mathbf{N} = [N_1, ..., N_N]^T$ represent, respectively, the frequency response of the transmitted signal, the channel and the noise at each OFDM subcarriers. Also, $diag(\mathbf{X})$ is a diagonal matrix having the elements of $\mathbf{X}$ in the main diagonal.

In the next Section, it will be introduced the classic and most popular used channel estimation techniques: the least-square (LS) and the linear minimum mean square error (LMMSE) estimators.

3.3.1 Least-Square Estimators

A simple method for channel estimation that does not require any CFR statistical information is the least-square (LS) approach where to estimate $H[n,k]$, denoted as $\hat{H}_{LS}$, it is necessary to compute [10]

$$\hat{H}_{LS_{k,n}} = \frac{Y_{k,n}}{X_{k,n}} = H_{k,n} + \frac{N_{k,n}}{X_{k,n}}. \tag{3.18}$$

In matrix notation, the above expression can be rewritten as

$$\hat{\mathbf{H}}_{LS} = \text{diag}(\mathbf{X})^{-1}\mathbf{Y} \tag{3.19}$$

Clearly, the LS estimator is equivalent to the ZF equalizer, and it has similar advantages and drawbacks. Although it constitutes a low complex algorithm, the major disadvantage comes from noise enhancement. Since LS estimators do not generally require any channel statistics, the estimation is not perfect enough, especially in scenarios of very fast channel variations where the system performance will significantly deteriorate [33]. Nevertheless, LS estimators are essential to obtain a first initial coarse channel estimation further refined by other estimators.

3.3.2 LMMSE Estimator

In a linear system model in the form of (3.17), the minimum mean square error MMSE channel estimator exploits the channel's correlations characteristics [34]. Therefore, the channel estimation, $\hat{H}_{LMMSE}$, is given by a Wiener filtering operation, that is

$$\hat{H}_{LMMSE_{k,n}} = \sum_{k,n} w_{k,n} \cdot \hat{H}_{LS_{k,n}}, \tag{3.20}$$

where k represents each n^{th} OFDM symbol subcarrier and $\hat{H}_{LS}$ the least-square estimator defined in (3.18). In matrix notation, the above expression can be rewritten as

$$\hat{H}_{LMMSE_{k,n}} = \mathbf{w}_{k,n}^{T} \hat{\mathbf{H}}_{LS_{k,n}}. \tag{3.21}$$

where $\mathbf{w}$ and $\hat{\mathbf{H}}_{LS}$ are column vectors. The optimum LMMSE coefficients can be given by

$$\mathbf{w}_{k,n} = \mathbf{R}_{k,n}^{-1} \mathbf{r}_{k,n}. \tag{3.22}$$

where the matrix $\mathbf{R}_{k,n}$ corresponds to the auto correlation covariance matrix between pilot subcarriers and vector $\mathbf{r}_{k,n}$ the cross correlation between between the desired channel estimation with the pilot set [34].

Although the LMMSE is more computational complex, its implementation can provide a better BER performance. Thus, a trade-off between the algorithm performance and complexity must be achieved since it is possible to obtain the same results, in certain channel conditions, applying only the LS approach [10].

3.3.3 Pilot Arrangement

There are several placement possibilities to adopt for pilot symbols. In the work presented in [35] the authors describe the pilot pattern as a *2D* lattice grid, Y, that maps the (time, frequency) plane as showed in Figure 3.3.

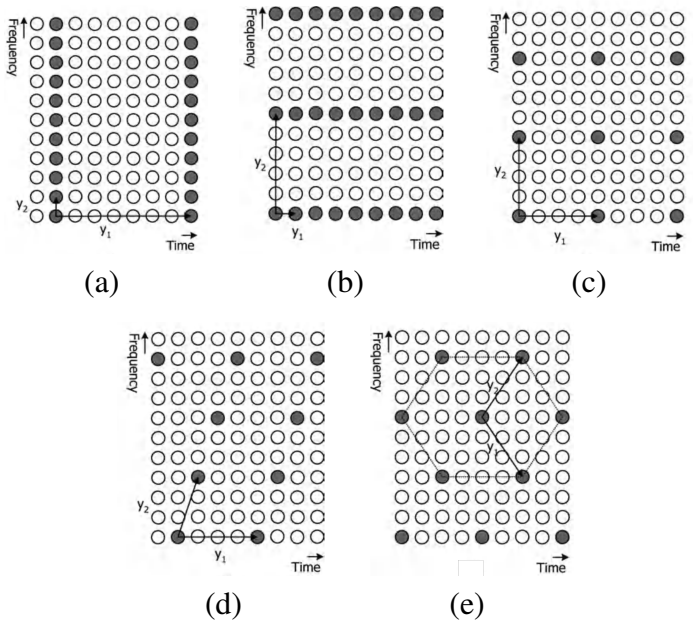

Figure 3.3: OFDM pilot allocation techniques where the grey dots correspond to the pilot's subcarriers and the blank to the data subcarriers [6]: **(a)** block-type **(b)** comb-type **(c)** rectangular grid **(d)** parallelogram-shaped grid **(e)** hexagonal grid

Commonly used in OFDM systems, the previous designs are represented by the following pattern models:

(i) the block-type pilot allocation, adopted in IEEE 802.11a/g/n standard, that corresponds to allocate pilots, in the frequency domain, into all subcarriers every y_{1_B} symbols and is denoted in (3.23).

$$\mathbf{Y}_{Block} = \begin{bmatrix} y_{1_B} & 0 \\ 0 & 1 \end{bmatrix}. \tag{3.23}$$

This technique is designed for slow-fading frequency selective channels when the OFDM symbols time duration is much smaller than the channel coherence time, i.e., significantly shorter than the inverse of the Doppler frequency [6];

(ii) the comb-type pilot allocation, used, for instance, in the IEEE 802.11a WLAN standard [9], corresponds to insert pilots, at predefined y_{2_C} subcarriers locations across all entire transmission time and can be expressed by (3.24).

$$\mathbf{Y}_{Comb} = \begin{bmatrix} 1 & 0 \\ 0 & y_{2_C} \end{bmatrix}. \tag{3.24}$$

Following this method, it is possible to resist fast channel time variations between OFDM symbols. However, it is crucial to guarantee the spacing between each pilot subcarriers much smaller than the channel coherence bandwidth for effective and accurate estimation.

In the remaining pilot allocation schemes, the pilots are scattered over time and frequency domain which enables a good tracking relationship between frequency selectivity and time variation of the wireless channel. Since the pilot's grid insertion is not made in all subcarriers or in fixed subcarriers across all the time, it is possible to achieve a better overall system performance by reducing the pilot density and thus improving the spectral efficiency. Nevertheless, the hexagonal grid pilot allocation can be addressed as the most efficient between the remaining patterns and is expressed by

$$\mathbf{Y}_{Hex} = \begin{bmatrix} y_{1_H} & y_{1_H} \\ -y_{2_H} & y_{2_H} \end{bmatrix}. \tag{3.25}$$

However in these types of arrangement it is important to guarantee the sampling theorem in order to avoid an aliasing effect to happen.

So far, an overview of several signal detection and channel estimators methods for OFDM were presented. Although the TIBWB-OFDM is an OFDM-based technique, its hybrid nature where the transmitted block can be seen, upon reception, as a block-based SC transmission type, precludes the direct extension of these methods to the TIBWB-OFDM system. Hence, the next Chapter will target these estimators analysis and study in the TIBWB-OFDM implementation environment.

4

Synchronization and Channel Estimation for TIBWB-OFDM

Contents

This Chapter contextualizes the necessary architecture to execute a testbed of the TIBWB-OFDM system described in Chapter 2. The problems of frame synchronization and channel estimation in a TIBWB-OFDM transmission are addressed, along with a study on equalizer performance working in imperfect channel estimation.

Chapter 4 is thus subdivided into four Sections. In Section 4.1 is made an analysis of the TIBWB-OFDM system model and the necessary modifications on it for a real wireless link scenario implementation, that includes the frame synchronization and channel estimation blocks. Section 4.2 presents the involved simulation environment parameters. Section 4.3 presents and discusses the results for the proposed frame synchronization algorithms, necessary for a reliable signal detection. Finally, Section 4.4 addresses the channel estimators and equalizers implementation, the final stage for fully decode the transmitted data correctly, presenting the overall BER system performance.

4.1 Proposed TIBWB-OFDM system model

The TIBWB-OFDM system model is presented in Figure 2.6. However, in order to perform signal synchronization and channel estimation tasks both transmitter and receiver schemes need to be reformulated. Briefly, the proposed system establishes a joint channel estimation and frame synchronization by padding a power amplified ZC preamble, that performs both assignments, to the TIBWB-OFDM block. The following two sub-sections explain with more detail the proposed transceiver architecture that provides answers to the described challenges.

4.1.1 Preamble-assisted transmitter

The transmitter architecture is now composed by a preamble generator, as depicted in Figure 4.2. The pilot allocation follows a block-type design (Section 3.3.3) due to the characteristics of the TIBWB-OFDM scheme where the packing of several OFDM symbols into a single block favors the adoption of the block-type pilot allocation strategy. On the other hand, if any of the other pilot allocation arrangements were used, the interleaving procedure would make it difficult to extract the pilot information upon reception.

The interleaved block vector, $\mathbf{s}_\pi$, (previously defined in (2.13)) is attached to the preamble sequence forming a new TIBWB-OFDM frame-block. Therefore, the obtained transmitted packet, whose schematic is depicted in Figure 4.1, is represented as

$$\mathbf{s_{frame}} = [\mathbf{s}_{p,N_p} | \mathbf{s}_{\pi,k}], \text{with } k = 1, ..., N_s\,, \tag{4.1}$$

where $\mathbf{s}_p$ constitutes the preamble generated sequence with length N_p.

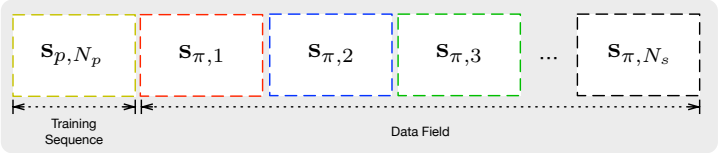

Figure 4.1: TIBWB-OFDM block frame structure adopted.

Finally, it is added the ZP vector to the transmitted assembled frame sequence, resulting in the complete transmitted block, $\mathbf{x}_n$, expressed as

$$\mathbf{x_n} = [\mathbf{s_{frame}} | 0_{(1\times N_{zp})}]_{1\times N_n}, \tag{4.2}$$

where vector $\mathbf{x_n}$ length is in the form of $N_n = N_{zp} + N_p + N_s \times N_{Symb}$.

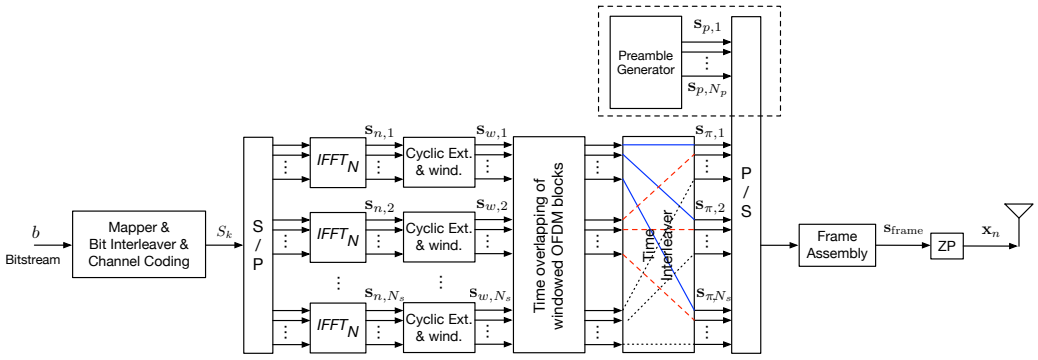

Figure 4.2: Preamble assisted TIBWB-OFDM transmitter modulation scheme.

For practical implementation, the preamble total size has the same size as a TIBWB-OFDM sub-block, that is, $N_p = N_{symb}$.

4.1.2 TIBWB-OFDM receiver with frame synchronization

Settling the transmitter schematic configuration, it is now vital to develop the receiver architecture. Hence, Figure 4.4 shows an additional new sub-system, referenced as Synchronization and Channel Estimators, essential to accomplish signal recovery synchronization, at a first instance, and only afterward, the frequency domain channel estimation and equalization. On the other hand, it is necessary to know the preamble transmitted sequence precisely. Thus, a stored preamble sequence constitutes a key element of the receiver structure.

Taking advantage from the ZC proprieties, a time-domain correlation operation can be performed between the preamble received signal and the known sequence. This technique will be the fundamental principle for the TIBWB-OFDM frame detection algorithm and follows the concepts presented in Section 3.1.1.

Figure 4.3 shows the step-by-step frame detection algorithm on the ZC preamble sequence. Hence, by auto-correlating the known preamble sequence the maximum correlation peak, P_{zc}, defined by (3.3) is expected to appear in the N_p sample (Figure 4.3a)). This value is extremely important since it will define the threshold percentage value for the receiver system markers and, therefore, affects the success / miss probability of detection.

Note that more than one peak may appear in dispersive channels situations due to late signal replicas arrival (Figure 4.3b)). Therefore, due to the channel taps delay, N_{delay}, after the threshold decision (Figure 4.3c)) it is necessary to develop a correction algorithm based on a moving window width factor, established to be equal to N_{delay}, and the marked threshold indexes (Figure 4.3d)).

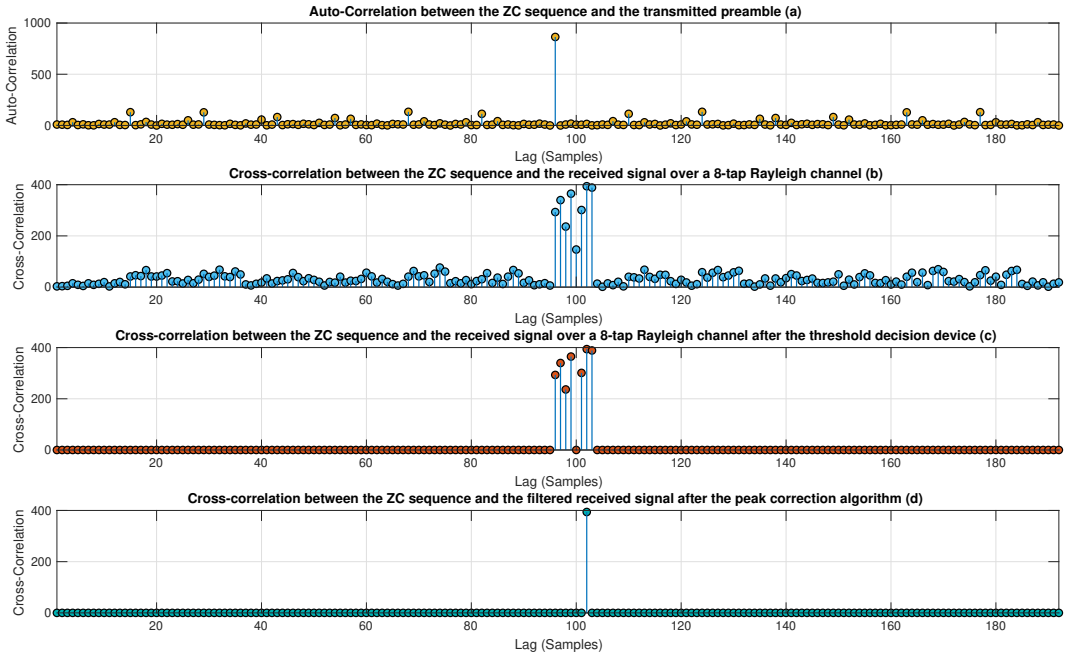

Figure 4.3: Frame detection algorithm procedure for the ZC preamble in the TIBWB-OFDM receiver system.

In Figure 4.3d), the unique amplitude peak marks the presence of the frame TIBWB-OFDM beginning. However, if we would encounter other high amplitude peaks where should not be expected, the algorithm acknowledges this event has a possible noise frame, rejecting the respective block.

4.1.3 TIBWB-OFDM receiver with channel estimation

After the frame synchronization, the same received preamble sequence is converted to the frequency domain, by means of a equal size FFT, in order to extract the channel state information (CSI). Three algorithms were developed and applied to the TIBWB-OFDM scheme:

Algorithm **A** - **Zadoff-Chu (ZC)** preamble based Channel Estimation;

Algorithm **B** - **Data** based Channel Estimation;

Algorithm **C** - Combined **ZC** and **Data** Channel Estimation.

In algorithm **A**, a LS estimator is applied (Section 3.3.1) to the received ZC sequence resulting in a low resolution estimated channel with equal length size to the preamble sequence. The estimated channel, $\widetilde{H}_k$, is therefore given by

$$\widetilde{H}_{k(zc),(N_p)} = \frac{FFT_{N_p}\{\widetilde{s_p}\}}{FFT_{N_p}\{s_p\}}, \tag{4.3}$$

where $\widetilde{s_p}$ represents the received preamble sequence.

It was admitted that the preamble sequence length is always larger than the channel impulse response (CIR), enabling the use of the IFFT to obtain an estimated channel with more resolution, that is

$$\widetilde{H}_{k(zc),(N_n)} = FFT_{Nn}\left\{IFFT_{Np}\left\{\widetilde{H}_{k,(N_p)}\right\}\right\}, \tag{4.4}$$

where $\widetilde{H}_{k,(N_n)}$ represents the estimated channel constituted by N_n samples.

Afterwards, the TIBWB-OFDM structure is composed by equalizers and block unformatting, i.e., block time de-interleaving, bit-deinterleaving, de-mapping, and channel decoding. Figure 4.4 shows the equalizers implementation specifically for the nonlinear IB-DFE type. In theory, if the desired receiver structure is a simple linear equalizer, then, only the TIBWB-OFDM unformatting is performed, obtaining the final estimated sequence, as a one iteration transceiver system.

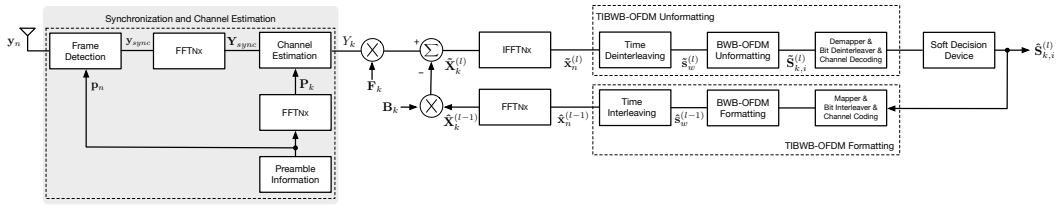

Figure 4.4: Preamble Assisted TIBWB-OFDM receiver modulation scheme.

However, if the IB-DFE is adopted it is possible to take advantage from the received and decoded data sequence to proceed to another estimation algorithm in each equalizer iteration. In other words, a second algorithm **B** can be designed, based on the estimated data by the ZC sequence, where in each iteration the channel is given by

$$\widetilde{H}_{k(data)} = \frac{Y_k^{(l)}}{\widehat{X}_k^{(l-1)}}, \tag{4.5}$$

where $\widehat{X}_k^{(l-1)}$ denotes the frequency domain signal estimated at the previous $(l-1)$ iteration.

On the other hand, a refined strategy for achieving successive better estimations is added to the IB-DFE scheme. Therefore, a third algorithm **C** based on the weighted mean between the ZC channel estimated sequence (algorithm **A**) and the data sequence estimated sequence (algorithm **B**) can be applied as follows

$$\widetilde{H}_{k(data+zc)} = \frac{\left(\frac{\widetilde{H}_{k(data)}}{\sigma^2_{(data)}} + \frac{\widetilde{H}_{k(zc)}}{\sigma^2_{(zc)}}\right)}{\left(\frac{1}{\sigma^2_{(data)}} + \frac{1}{\sigma^2_{(zc)}}\right)}, \tag{4.6}$$

where $\sigma^2_{(zc)}$ and $\sigma^2_{(data)}$ represents individually the mean square error between the estimated ZC and data sequence, respectively, and the original channel. This relation is given by

$$\sigma^2_{(chu/data)} = \mathbf{E}\left\{\left|H_k - \widetilde{H}_{k(chu/data)}\right|^2\right\}. \tag{4.7}$$

On the other hand, all three developed algorithms can explore a direct application from the LMMSE estimator.

4.2 Setup configurations for the experimental study

The parameters for the TIBWB-OFDM wireless SISO model simulations are, unless otherwise stated, defined as:

(i) **Preamble sequence**: ZC preambles are implemented with a root element number of $n = 34$. This specific root index, used in the LTE systems, show a good correlation performance and also have a low frequency-offset sensitivity, which give robustness to the synchronization detection algorithm [29]. The preamble length is $N_p = 96$ where the generated ZC sequence length is $N_{ZC} = 95$ being padded a zero value in the last sample to complete the total preamble length.

(ii) **TIBWB-OFDM block**: The frame size adopted is identical for both synchronization and channel estimation simulations. Hence, the transmitted frame is formed by $N_s = 42$ OFDM blocks constituted of $N = 64$ subcarriers, with the symbols assigned to each subcarrier being from a QPSK modulation under a Gray coding rule. The windowing of the OFDM component blocks is carried using a SRRC window with roll-off of $\beta = 0.5$. Therefore, the total frame block length is $N_{total} = (N_s - 1) \times N \times (1 + \beta) + N_p = 4032$ samples where the first block of 96 samples corresponds to the preamble sequence and the remaining 41 blocks to the data frames sequences. Channel coding and bit-interleaving were also used to achieve a better system performance. Hence, a $(128, 64)$ short low-density parity-check (LDPC) code and bit-interleaving were applied over 10 consecutive coded words.

(iii) **Wireless channel model**: Tests were carried over a Rayleigh channel due to its features of characterizing the signal interference in non-LoS environments, constituting a reliable approximation for wireless links. To test the behavior of the TIBWB-OFDM channel and synchronization estimators we considered two severe Rayleigh channel scenarios, an 8 and 32 symbol-spaced multipath channel echos (channel taps) with uncorrelated Rayleigh fading, that were used to test the frame detection probability error and the channel estimators BER performance respectively.

4.3 Frame Synchronization results

The following work attempt to confront the frame detection synchronization results as the primary challenge to compensate for channel interference effects.

The In-phase and Quadrature complex value representation of the constant amplitude ZC sequence is depicted in Figure 4.5a. It is visible that there is a perfect circular configuration, which after adding an AWGN component, will spread the generated samples randomly, as shown in Figure 4.5b.

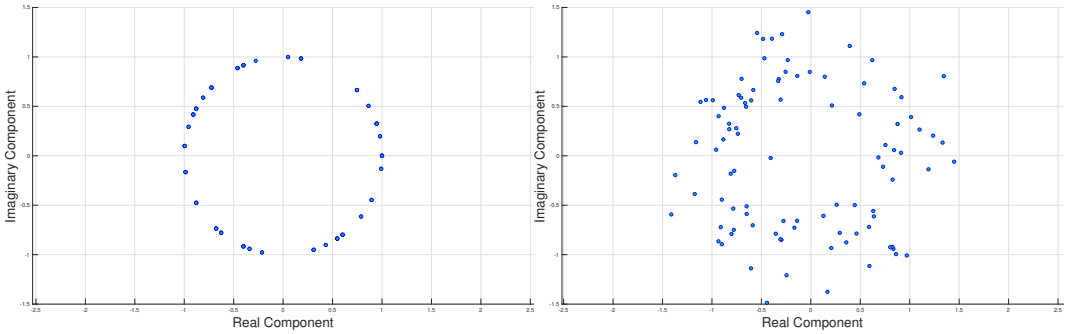

(a) (b)

Figure 4.5: Generated synchronization signal (a) and received synchronization signal with AWGN (b).

Taking advantage from the ZC proprieties, a time-domain correlation operation can be performed between the preamble signal affected by the AWGN and the known sequence. This technique will be the fundamental principle for the TIBWB-OFDM frame detection algorithm. The results are presented in Figure 4.6a). These allow to confirm that it is achievable to detect the synchronization sequence by noticing the high peak amplitude value centered on the middle correlation sample, meaning that both correlated signals match, i.e., both sequences are identical, which signals the frame beginning. On the other hand, Figure 4.6b) shows the cross-correlation between a ZC sequence and a data frame where it may be observed successive low coefficients values of the cross-correlation operation, implying that the transmitted signal does not include the desired information.

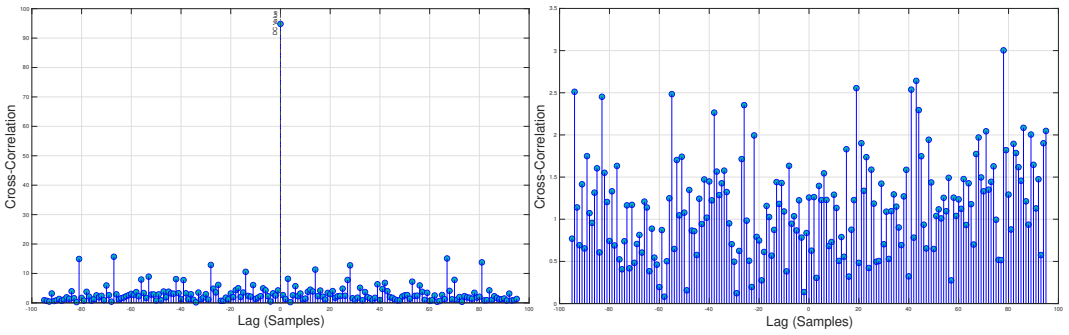

(a) (b)

Figure 4.6: Correlation: (a) between the known ZC synchronization and the received ZC signal with AWGN, and (b) between a random received data signal with AWGN.

It is thus clear that it is possible to benefit from the high dominant correlation peak to detect the frame beginning of a TIBWB-OFDM block. Accurate detection can be achieved by implementing a threshold methodology. Nevertheless, this decision device implementation is not straightforward due to the wireless channel

multipath effect. So, to achieve a good probability performance, the threshold position cannot be fixed, meaning that, to find the optimum index value, a dynamic algorithm that fluctuates depending on the transmitted correlation preamble amplitude peak must be taken into account. Increasing power to the ZC sequence could also minimize the error detection probability due to the more enhanced amplitude correlation peaks. Therefore, a 3 and 6 dB power amplification performance is also explored, i.e., the average power of the transmitted ZC sequence is 3 or 6 dB higher than the average TIBWB-OFDM data power block. On the other hand, the channel estimators' performance, addressed in the next Section, will also explore this feature. Hence, it is reasonable to benefit from this attribute and jointly adopt it for both tasks.

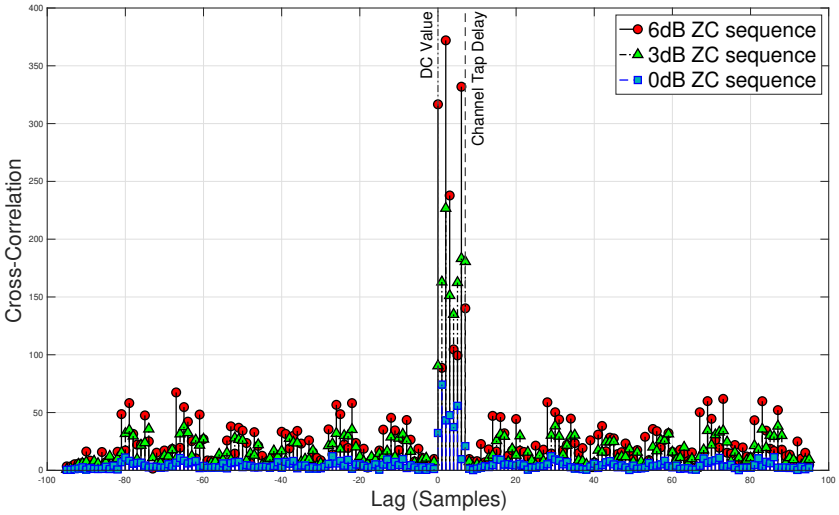

Figure 4.7: Cross-correlation between the known ZC synchronization signal and the received preamble sequence affected by a 8-tap Rayleigh channel.

Figure 4.7 shows the referred channel interference effects in a Rayleigh Channel with 8 symbol-spaced multipath channel echos. It is visible that the channel taps delay affect, with several repeated high dominant peak components being observed. So, instead of seeing a single peak centered on the middle sample, it is expected to see N_{delay} replicas, with attenuated amplitude values.

4.3.1 Threshold Decision Device

The following simulations aim to evaluate and acquire the best threshold index number that reduces the miss frame probability. Therefore, 700 data frames, i.e, TIBWB-OFDM blocks, are randomly interleaved with 300 AWGN frame samples equally sized from the data blocks. The cross-correlation of the used ZC sequence with the transmitted and received signals is shown respectively in Figure

4.8 and 4.9, for a small simulation window time slot, composed of the first seven TIBWB-OFDM frames and three noise frames. It is important to enhance that all the preamble signals are identical which reflects on the same transmitted visible high correlation peak amplitude.

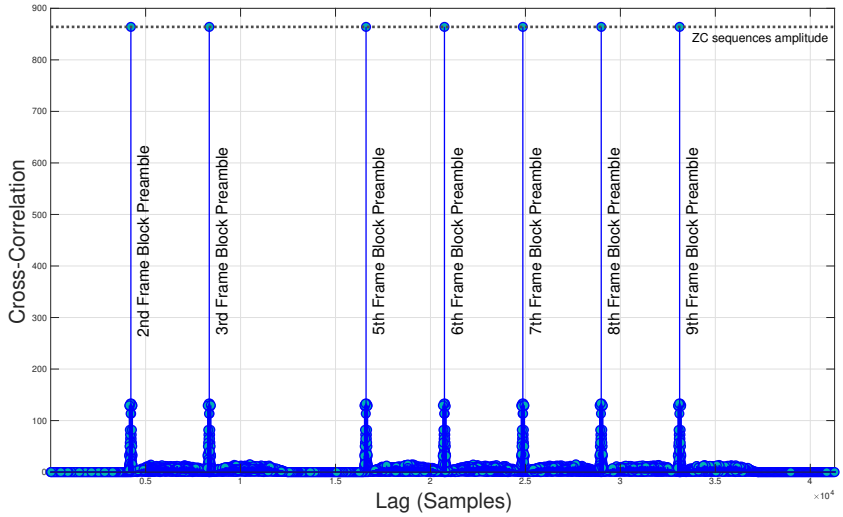

Figure 4.8: Cross-correlation of the ZC sequence with transmitted signal for a time window slot composed by 7 data blocks and 3 noise frames.

It is visible, by analyzing the previous results, the presence of AWGN frames, in the first 4032 samples, between the 3^{rd} and 5^{th} TIBWB-OFDM frame and after the 9^{th} data frame block. Also, in Figure 4.9, we visualize the channel fading effects in the transmitted sequence, i.e., the presence of lower and repeated amplitude correlation peaks that should mark the frame beginning.

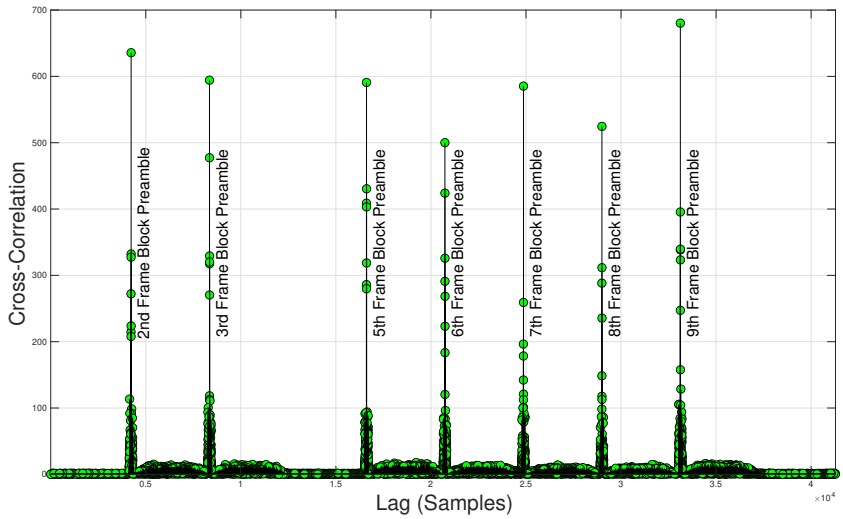

Figure 4.9: Cross-correlation of the ZC sequence with the received signal over a 8-tap Rayleigh channel, for a time window slot composed by 7 data blocks and 3 noise frames.

As referred, one of the critical performance variables is the selection of the threshold cross-correlation level used to indicate the beginning of a new frame. Hence, the used value should be as accurate as possible to achieve an acceptable frame detection that will subsequently influence the BER system performance and error awareness. So, Figure 4.10 shows the probability of correct detection as a function of the setup threshold level, defined as a percentage of the maximum value of the ZC auto-correlation, P_{zc}.

According to Figure 4.10 the threshold value should be selected in the range of $25\% - 30\%$ of the P_{zc}, in which it can be observed that the probability of correct detection is almost 1.

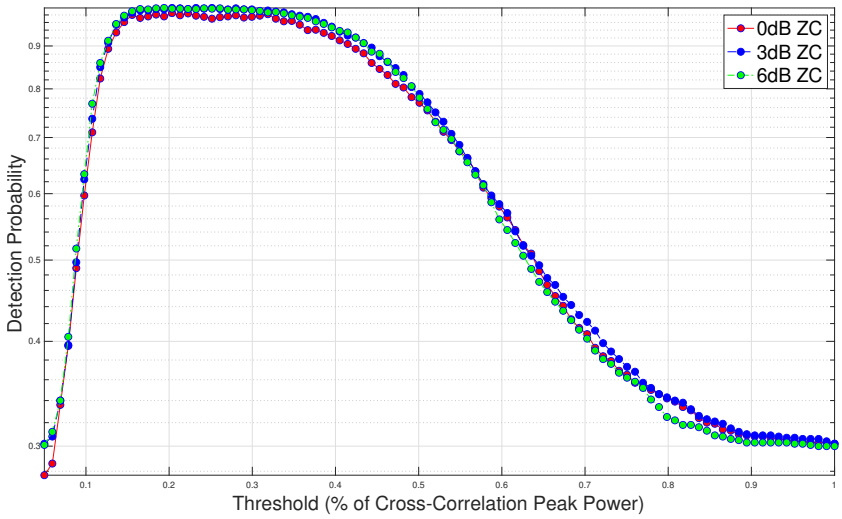

Figure 4.10: Correct frame detection probability as function of the cross correlation's threshold value for peak detection.

Results on Figure 4.10 were obtained keeping fixed the AWGN power, while varying the ZC sequence power showing that this is almost independent from the SNR. When the threshold parameter is near the maximum of the auto correlation P_{zc} no data frames are detected. This is due to the fact that the signal suffers from fading (i.e., variable gain attenuation due to multipath effect), with the cross-correlation value hardly reaching the P_{zc} value. In this case since almost all frames are marked as noise, the probability of right detection is 30% corresponding to the fraction of noise frames sent.

On the contrary, by settling the threshold too low, the opposite effect occurs with almost all frames being detected as data. Here, the coexisting noise peaks combined with those of the data sequences, both above the threshold make it impossible to detect a single peak value causing the frame recognition task very challenging to accomplish. However, in this scenario, a noteworthy difference is visible between the non-amplified ZC sequences and the remaining sequences. Since the threshold

is defined as a percentage of P_{zc}, for the 3 dB and 6dB cases, the threshold is much higher precluding any noise frame to be marked as data, and, thus, the probability of a correct detection is above 30%.

At last, a study about the amplified ZC preamble sequences is performed for different levels of noise power. Figure 4.11, shows the referred simulation for a 3 dB amplified preamble.

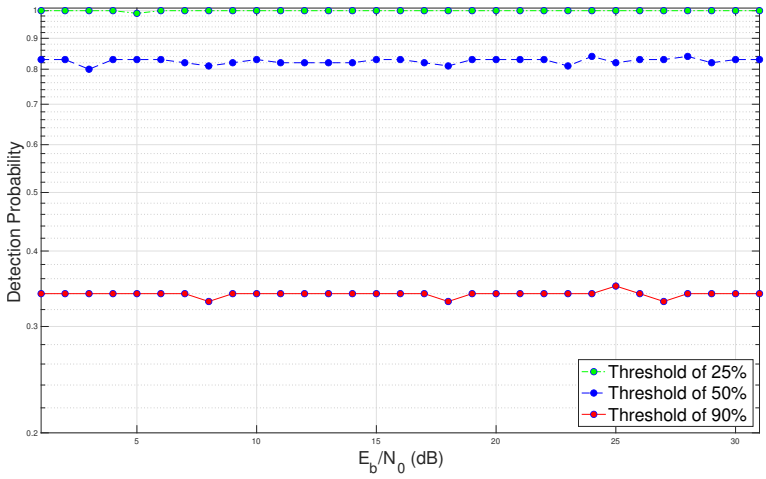

Figure 4.11: Frame detection probability for several SNR values.

From the analyses of these results, we conclude that the detection probability is highly insensitive to SNR fluctuations. So, once again, the threshold decision is the crucial factor that defines the synchronization overall performance.

4.4 Channel Estimation results

After solving the frame synchronization problem, it is now necessary to face another challenge caused by the channel, i.e., the multipath channel effect and noise interference that destroy the signal information. In order to retrieve information from the received signal, this has to be equalized, and for that, accurate CSI should be available.

Therefore, the subsequent simulations seek to evaluate the BER performance results of the TIBWB-OFDM modulation scheme in a set condition without the perfect channel state knowledge and compare them with the case of perfect CSI.

4.4.1 TIBWB-OFDM *vs* TIBWB-OFDM with Channel Estimation

Figure 4.12 presents the TIBWB-OFDM BER performances, while applying ZC sequences as preamble assisted sequences in order to perform channel estimation. For a low computational approach, the LS estimator was chosen as the estimation

algorithm where the first goal was to find how the ZC sequences would perform in channel estimation for TIBWB-OFDM modulation with linear equalization. As referred, the LMMSE estimation can replace the implemented estimator. However, carried experiences have shown that in terms of complexity vs performance the algorithm did not justify it application. Therefore, we opted to present the results regarding only the LS estimator.

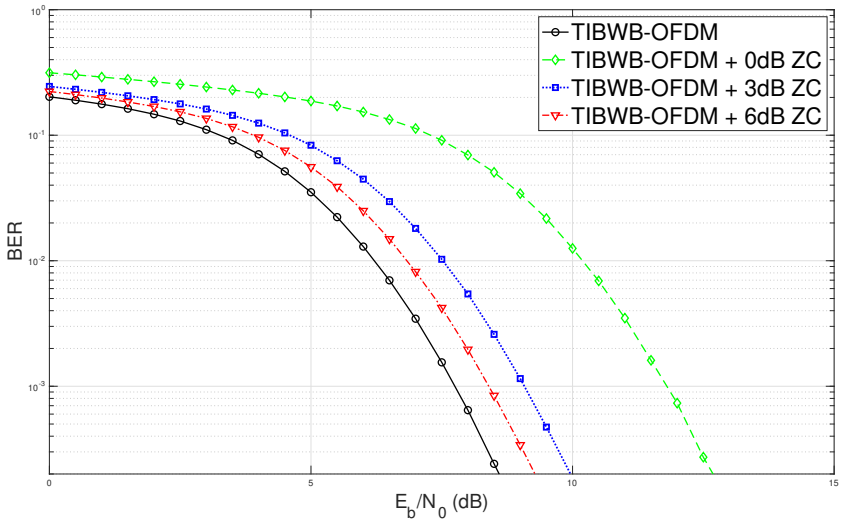

Figure 4.12: BER results for TIBWB-OFDM over a dispersive channel employing algorithm **A** techniques for a ZC preamble sequence with power amplification.

Although the optimal channel state information is not possible, a good performance approximation comes with the price of a necessary increase power of the preamble sequence. Having has reference the average power of the TIBWB-OFDM data block, we tested 3 situations, were the appended ZC preamble was sent with the same power as data (i.e. 0dB case), or +3 dB or +6 dB.

The system performance shows an evident gain between a subtle power amplification of plus 3 dB and a normal ZC sequence. Also, between 3 dB and 6 dB amplification, it is possible to achieve a slight improvement, almost reaching the optimal TIBWB-OFDM performance assuming perfect synchronization and channel estimation.

It is essential to highlight that although it is wasted additional power for good system performance, it is only applied to the preamble of the BWB-OFDM block, which reflects in an approximate 2% of additional wasted total system power in the 3 dB scenario, and 5% in the 6 dB scenario. Hence, it can be concluded that it is not critical to increase our preamble power since the total overall efficiency power calculation is weighted on the data frame and not on the preamble sequence.

4.4.2 *Channel Estimation* in TIBWB-OFDM with Iterative Frequency Domain Equalizers

Aiming to achieve an even better estimation of the original bit-stream, another TIBWB-OFDM approach was based on applying a frequency domain iterative equalizer in the receiver system, more specifically the IB-DFE with algorithm C applied. Therefore, the next simulations, depicted in Figure 4.13, 4.14 and 4.15, show the set of results, concerning the BER performance.

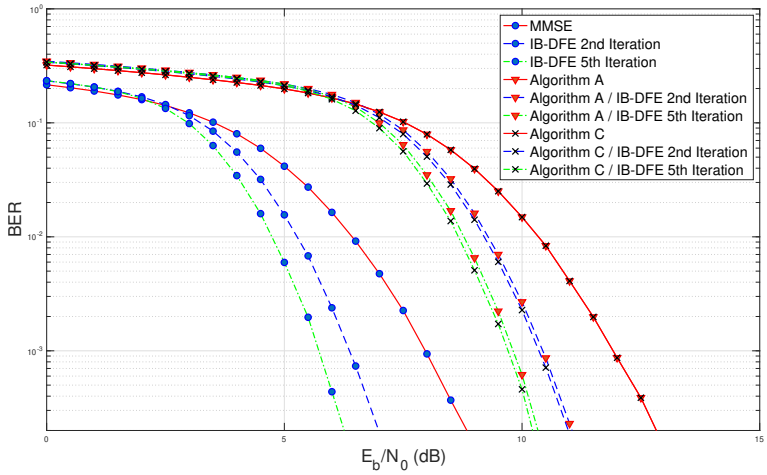

Figure 4.13: BER results for TIBWB-OFDM with IB-DFE over a dispersive channel employing algorithm **C** for a ZC preamble sequence with 0 dB power amplifier.

It should be reasonable to think that for low SNR values, the channel would maintain massive influence in the mean square error calculation, and for high SNR values, the opposite effect should happen. It should also be expected to achieve at each IB-DFE iteration a gradual better performance.

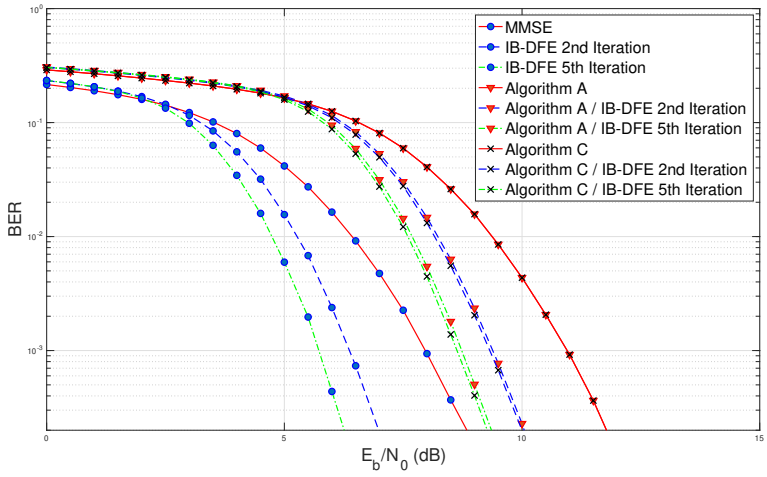

Figure 4.14: BER results for TIBWB-OFDM with IB-DFE over a dispersive channel employing algorithm **C** for a ZC preamble sequence with 3 dB power amplifier.

However, we can start to realize, based on the first BER results for a ZC sequence with no power amplification, that the fine estimation does not significantly affect the overall system performance. This can be justified by calling the good performance of ZC on dispersive channels and how ineffective the interferences affect the preamble sequence. Also, the data does not present these good characteristics for channel estimation. So, the algorithm's estimated weight is enhanced by the first estimation, performed by the ZC preamble, i.e., by the algorithm A.

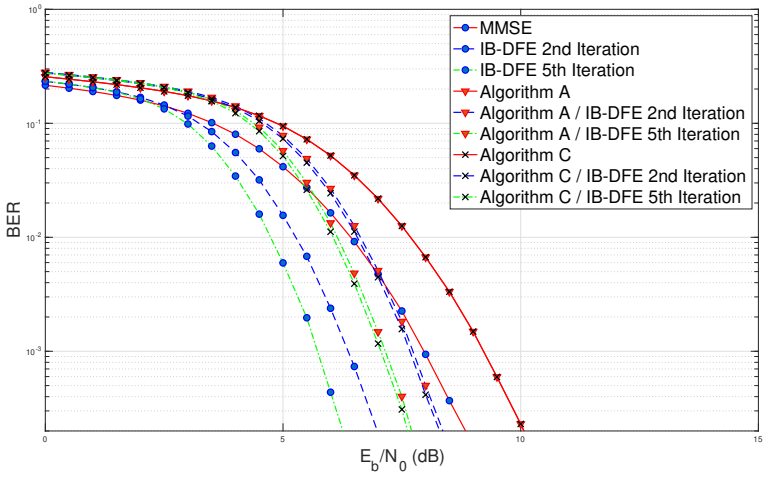

Figure 4.15: BER results for TIBWB-OFDM with IB-DFE over a dispersive channel employing algorithm **C** for a ZC preamble sequence with 6 dB power amplifier.

A final note that needs to be addressed is that although a slight performance increase is achieved, the algorithm C complexity does not justify this extra estimation procedure. From the previous conclusions, it is expected that this effect will maintain in the following BER performances where amplified preamble sequences are used. It is clear that the IB-DFE receiver shows some performance evolution form iteration to iteration. However, TIBWB-OFDM receiver gain is more pronounced between the 1^{st} and 2^{nd} IB-DFE iteration and the following iterations until the 5^{th} only a substantial gain is achieved.

5

Conclusions

The TIBWB-OFDM modulation's scientific research has been focused on evaluating the BER, PAPR performances and spectral efficiency for wireless channels that were admitted as *a priori* known, hence, they were considered as perfectly estimated and synchronization errors did not occur.

The developed work constitutes a new step to provide an insight on channel estimation and frame detection algorithms that could perform well in disperse channel conditions for the TIBWB-OFDM scheme. This thesis work, shows that the developed estimators by means of block-type preamble assisted frames can provide a similar BER system performance in comparison with the true channel state information performances due to the careful choice of the preamble sequences. So, it is useful to implement the pilot design based on Zadoff-Chu sequences due to their good correlation characteristics, and is proven that they are able to jointly execute channel and synchronization estimation effectively in our hybrid modulation architecture. Nevertheless, it is necessary to guarantee that the preamble power block is amplified in scenarios of 3 dB or 6 dB which is not critical, since the preamble represents only one block from the complete total signal frame. Therefore, a proof of concept of how the studied modulation scheme should perform in a real world environment is established in this thesis.

Considering the obtained results in this work, future developments should involve the study of frequency synchronization error for a OFDM-based systems and the type of cancellation methods that could perform well in our hybrid modulation scheme. It is also feasible to implement the proposed synchronization and channel estimators in a practical real environment, i.e., in a testbed software defined radio (SDR) development for the TIBWB-OFDM system. An interesting future work possibility is the extension of the SISO system, studied in this thesis, into a MIMO transceiver scheme implementation for the TIBWB-OFDM modulation, which will present different varied challenges.

Bibliography

[1] J. Nunes, P. Bento, M. Gomes, R. Dinis, and V. Silva, "Block-windowed burst OFDM: A high-efficiency multicarrier technique," *Electronics Letters*, vol. 50, no. 23, pp. 1757–1759, 2014.

[2] T. Fernandes, M. Gomes, V. Silva, and R. Dinis, "Time-Interleaved Block-Windowed Burst OFDM," *IEEE Vehicular Technology Conference*, 2016.

[3] T. Fernandes, A. Pereira, M. Gomes, V. Silva, and R. Dinis, "A new hybrid multicarrier transmission technique with iterative frequency domain detection," *Physical Communication*, vol. 27, pp. 7–16, 2018. [Online]. Available: https://doi.org/10.1016/j.phycom.2017.12.014

[4] F. Conceição, M. Gomes, V. Silva, and R. Dinis, "Highly efficient TIBWB-OFDM waveform for broadband wireless communications," *IEEE Vehicular Technology Conference*, 2020.

[5] R. Prasad, *OFDM for Wireless Communications Systems*. Artech House, 2004.

[6] T.-D. Chiueh, P.-y. Tsai, and I.-W. Lai, *Baseband Receiver Design for Wireless MIMO-OFDM*. Wiley-IEEE Press, 2012.

[7] M. Vaezi, Z. Ding, and H. Vincent Poor, *Multiple access techniques for 5G wireless networks and beyond*, 2018.

[8] V. Tarokh, *New Directions in Wireless Communications*. Springer Publishing Company, Incorporated, 2009.

[9] C. C. J. K. Man-on Pun, Michele Morelli, *Multi-Carrier Techniques For Broadband Wireless Communications: A Signal Processing Perspective*. Imperial College Press, 2007.

[10] M. K. Ozdemir and H. Arslan, "Channel Estimation for Wireless OFDM Systems," *IEEE Communications Surveys and Tutorials*, 2007.

[11] X. Yin and X. Cheng, *Propagation Channel Characterization, Parameter Estimation, and Modeling for Wireless Communications*. Wiley-IEEE Press, 2016.

[12] C. A. Balanis, *Antenna Theory: Analysis and Design*. Wiley, 2016.

[13] A. Goldsmith, *Wireless Communications*. Cambridge University Press, 2005.

[14] M. S. John G. Proakis, *Digital Communications*. McGraw-Hill, 2008.

[15] Y. Rahmatallah and S. Mohan, "Peak-to-average power ratio reduction in ofdm systems: A survey and taxonomy," *IEEE Communications Surveys and Tutorials*, vol. 15, no. 4, pp. 1567–1592, 2013.

[16] S. Haykin, *Digital Communication Systems*. Wiley, 2014.

[17] N. Souto, R. Dinis, A. Correia, and C. Reis, "Interference-Aware Iterative Block Decision Feedback Equalizer for Single-Carrier Transmission," *IEEE Transactions on Vehicular Technology*, vol. 64, no. 7, pp. 3316–3321, 2015.

[18] B. N. Benvenuto, R. Dinis, D. Falconer, and S. Tomasin, "Single Carrier Modulation With Nonlinear Frequency Domain Equalization," *Proceedings of the IEEE*, vol. 98, no. 1, pp. 69–96, 2010.

[19] T. Fernandes, *Time-Interleaved BWB-OFDM with Iterative FDE (MSc thesis)*. Coimbra University, Coimbra, 2015.

[20] M. Speth, S. A. Fechtel, G. Fock, and H. Meyr, "Optimum receiver design for wireless broad-band systems using OFDM-part I," *IEEE Transactions on Communications*, vol. 47, no. 11, pp. 1668–1677, 1999.

[21] D. P. Travis F. Collins, Robin Getz and A. M. Wyglinski, *Software-Defined Radio for Engineers*. Artech House mobile communications series, 2018.

[22] T. M. Schmidl and D. Cox, "Robust frequency and timing synchronization for OFDM," *IEEE Transactions on Communications*, vol. 45, no. 12, pp. 1613–1621, 1997.

[23] C. You, H. Horng, and J.-Y. Zhang, "Timing Synchronization for OFDM-based wireless networks," 2001.

[24] C. D. Parekha and J. M. Patel, "Overview on synchronization in OFDM systems," *Proceedings - 2016 International Conference on Advances in Computing, Communication and Automation, ICACCA 2016*, 2016.

[25] A. Aboltins and D. Klavins, "Synchronization for OFDM-based communication system: a brief overview," in *Riga Technical University 50th International Scientific Conference*, 2009.

[26] F. Khan, *LTE for 4G Mobile Broadband*. Cambridge University Press, 2009.

[27] D. C. CHU, "Polyphase codes with good periodic correlation properties (Corresp.)," *IEEE transactions on Information Theory*, 1972.

[28] Erik Dahlman, Stefan Parkvall, and J. Skold, *4G, LTE-Advanced Pro and The Road to 5G*, 2016.

[29] S. Sesia, I. Toufik, and M. Baker, "LTE - The UMTS Long Term Evolution: From Theory to Practice," 2011.

[30] M. Hua, M. Wang, K. W. Yang, and K. J. Zou, "Analysis of the frequency offset effect on Zadoff-Chu sequence timing performance," *IEEE Transactions on Communications*, vol. 62, no. 11, pp. 4024–4039, 2014.

[31] S. Ohno, E. Manasseh, and M. Nakamoto, "Preamble and pilot symbol design for channel estimation in OFDM systems with null subcarriers," *Eurasip Journal on Wireless Communications and Networking*, vol. 2011, no. 1, p. 2, 2011. [Online]. Available: http://jwcn.eurasipjournals.com/content/2011/1/2

[32] K. Fazel and S. Kaiser, *Multi-Carrier and Spread Spectrum Systems: From OFDM and MC-CDMA to LTE and WiMAX*, Wiley, Ed. Wiley, 2008.

[33] C.-x. Wang, B. Jiao, M. Wen, X. Cheng, and Z. Zhao, "Channel Estimation Schemes for IEEE 802.11p Standard," *IEEE Intelligent Transportation Systems Magazine*, 2013.

[34] H. Wei, Y. Huang, T. Zhang, and L. Li, "An Universal MMSE Channel Estimator for OFDM Receiver," *Wireless Personal Communications*, vol. 94, no. 3, pp. 659–673, 2017.

[35] M. J. Fernandez-Getino Garcia, S. Zazo, and J. M. Paez-Borrallo, "Pilot patterns for channel estimation in OFDM," *Electronics Letters*, 2000.

[36] N. Benvenuto and S. Tomasin, "Iterative design and detection of a DFE in the frequency domain," *IEEE Transactions on Communications*, vol. 53, no. 11, pp. 1867–1875, 2005.

[37] F. Conceição, *New Hybrid Modulation Techniques for Future Generations of Communications (MSc thesis)*. Coimbra University, Coimbra, 2019.

[38] J. J. van de Beek, O. Edfors, M. Sandell, S. K. Wilson, and P. O. Borjesson, "On channel estimation in OFDM systems," *IEEE Vehicular Technology Conference*, vol. 2, no. 1, pp. 815–819, 1995.

[39] J.-J. Van De Beek, M. Sandell, and P. O. Börjesson, "On synchronization in OFDM systems using the cyclic prefix," *Division of Signal Processing, Lulea University of Technology, Lulea, Sweden*, pp. 1–5, 1996.

[40] F. Nunes, *Sistema OFDM multi-símbolo : Uma abordagem multiportadora eficiente (MSc thesis)*. Coimbra University, Coimbra, 2014.